INVESTIGATIONS ON THE ROLE OF ATMOSPHERIC BOUNDARY LAYER DYNAMICS IN MODULATING THE AIR QUALITY

by

AMRUTHA M. S.

(2015 - 20 - 006)

THESIS

Submitted in the partial fulfilment of the

requirements for the degree of

BSc.-MSc. (Integrated) Climate Change Adaptation

Faculty of Agriculture

Kerala Agricultural University

ACADEMY OF CLIMATE CHANGE EDUCATION AND RESEARCH

VELLANIKKARA, THRISSUR – 680 656

KERALA, INDIA

2020

DECLARATION

I, Amrutha M. S., (2015-20-006) hereby declare that this thesis entitled **"INVESTIGATIONS ON THE ROLE OF ATMOSPHERIC BOUNDARY LAYER DYNAMICS IN MODULATING THE AIR QUALITY"** is a bonafide record of research work done by me during the course of research and the thesis has not previously formed the basis for the award to me of any degree, diploma, associateship, fellowship or other similar title, of any other University or Society.

Vellanikkara, **Amrutha M. S.**

(2015-20-006)

CERTIFICATE

Certified that this thesis entitled **"INVESTIGATIONS ON THE ROLE OF ATMOSPHERIC BOUNDARY LAYER DYNAMICS IN MODULATING THE AIR QUALITY"** is a record of research work done independently by Ms. Amrutha M. S. under my guidance and supervision and that it has not previously formed the basis for the award of any degree, diploma, fellowship or associateship to her.

Vellanikkara

Dr. P. O. Nameer
(Chairman, Advisory committee)
Special Officer
Academy of Climate Change Education and Research (ACCER)
Kerala Agricultural University (KAU)
Vellanikkara, Thrissur

CERTIFICATE

We, the undersigned members of the advisory committee of Ms. Amrutha M. S., a candidate for the degree of BSc.-MSc. (Integrated) Climate Change Adaptation, agree that the thesis entitled **"INVESTIGATIONS ON THE ROLE OF ATMOSPHERIC BOUNDARY LAYER DYNAMICS IN MODULATING THE AIR QUALITY"** may be submitted by Ms. Amrutha M. S., (2015-20-006) in partial fulfilment of the requirements for the degree.

Dr. P. O. Nameer
(Chairman, Advisory committee)
Special Officer
Academy of Climate Change Education and Research
Kerala Agricultural University
Vellanikkara, Thrissur

Dr. K. Krishna Moorthy
(Member, Advisory committee)
Distinguished visiting scientist
Centre for Atmospheric and Oceanic Sciences
Indian Institute of Science
Bengaluru

Dr. Anand N.
(Member, Advisory committee)
Centre for Atmospheric and Oceanic Sciences
Indian Institute of Science
Bengaluru

Dr. Kunhamu T. K.
(Member, Advisory committee)
Professor and Head
Department of Silviculture and Agroforestry
College of Forestry
Kerala Agricultural University
Vellanikkara, Thrissur

EXTERNAL EXAMINER

ACKNOWLEDGEMENT

I would like to express my sincere thanks to my guide Dr. K. Krishna Moorthy, Distinguished Visiting Scientist, Centre for Atmospheric and Oceanic Sciences (CAOS), Indian Institute of Science (IISc), Bengaluru for having given me an opportunity to do this research, valuable guidance and suggestions throughout my work. I feel deeply honoured to work under his supervision.

I dedicate my grateful thanks to the Chairman of the Advisory Committee Dr. P. O. Nameer, Special Officer, ACCER, KAU for his advice, encouragement, and moral support.

I respectfully thank Prof. S. K. Satheesh, Professor, CAOS, and Chairman, Divecha Centre for Climate Change (DCCC), IISc, Bengaluru for his useful suggestions and support. I feel privileged to work in his lab.

I extend my heartfelt gratitude to Dr. Anand N., CAOS, IISc, Bengaluru for his valuable and timely suggestions, useful discussions, constant support, encouragement and paving better path towards the successful completion of my thesis.

I extend my gratefulness to Dr. Kunhamu T. K., Professor and Head, Department of Silviculture and Agroforestry, College of Forestry, KAU for his advice and suggestions.

Next, I acknowledge Dr. Manoj M. R., Project Scientist, DCCC, IISc, Bengaluru for his suggestions.

I take this opportunity to thank everyone at DCCC especially, Mr. Arun, Mrs. Arya, Ms. Veena, Ms. Devika, Ms. Sreemayi, Ms. Greeshma, Ms. Sreepriya, Mr. Aditya, Mr. Thashwin, and Mr. Abhishek, for their help, love and support throughout the tenure.

My special thanks are extended to my friends Ms. Gopika and Ms. Gayathri for their help, encouragement and support. They always stood beside me during all the happy and hard moments.

My sincere thanks to all my dear amazing friends Exemiers – 2015, for all the love and support throughout the college days.

I would like to extend my gratitude towards all the students, teaching and non-teaching staffs of ACCER for all the support during my entire college life.

I am indebted to my parents and brother, for their patience, selfless love, constant encouragement, valuable prayers and blessings showered upon me.

Finally, above all, I would like to thank almighty for being my strength and giving me knowledge and ability to complete this work successfully.

Amrutha M. S.

TABLE OF CONTENTS

LIST OF TABLES

LIST OF FIGURES

LIST OF ABBREVIATIONS

3D	Three dimensional
AAOD	Absorbing aerosol optical depth
ABL	Atmospheric boundary layer
ACE	Aerosol Characterisation Experiment
AERONET	Aerosol Robotic Network
AE – 33	Aethalometer – 33
AOD	Aerosol optical depth
AR	Assessment report
ARIFNET	Aerosol Radiative Forcing over India NETwork
AS	Arabian sea
AT	Air temperature
ATEX	Atlantic Trade wind Experiment
ATN	Attenuation
BC	Black carbon
BoB	Bay of Bengal
CBL	Convective boundary layer
CCN	Cloud condensation nuclei
CI	Capping inversion
DALR	Dry adiabatic lapse rate
ELR	Environmental lapse rate
EM	Electromagnetic radiation
EZ	Entrainment zone
FA	Free atmosphere
FAO	Food and Agriculture Organisation
FGGE	First GARP Global Experiment
GATE	GARP Atlantic Tropical Experiment

ICARB	Integrated Campaign for Aerosols, Gases and Radiation Budget
IGBP	International Geosphere Biosphere Program
IISc	Indian Institute of Science
IMAP	Indian Middle Atmosphere Program
IMD	India meteorological Department
INDOEX	Indian Ocean Experiment
IPCC	Intergovernmental Panel on Climate Change
IRGASON	Integrated Open Path Gas Analyser and Sonic Anemometer
ISM	Indian Summer Monsoon
ISMEX-33	Indo Soviet Monsoon Experiment – 33
ISRO	Indian Space Research Organisation
LT	Local time
MABL	Marine atmospheric boundary layer
ML	Mixed layer
MLH	Mixed layer height
MONEX -79	Monsoon Experiment
NBL	Nocturnal boundary layer
PBL	Planetary boundary layer
RCP	Representative Concentration Pathway
RF	Radiative forcing
RH	Relative humidity
RL	Residual layer
SBL	Stable boundary layer
SCAR	Smoke, cloud and Radiation Experiment
SL	Surface layer
SW_{down}	Downwelling short wave solar radiation
SWAAMI	South West Asian Aerosol Monsoon Interaction

TARFOX	Tropospheric Aerosol Radiative Forcing Observational Experiment
TOGA	Tropical Ocean Global Experiment
TKE	Turbulence kinetic energy
VC	Ventilation coefficient
WD	Wind direction
WS	Wind speed

LIST OF VARIABLES

t	Time
$u(t), v(t)$	Instantaneous wind speed in x and y directions
$\bar{u}$, $\bar{v}$	Mean wind speed in x and y directions
$\acute{u}$, $\acute{v}$	Turbulent part of instantaneous wind speed in x and y directions
θ	Potential temperature
T	Temperature
P	Pressure
C_p	Specific heat at constant pressure
z	Altitude
P_o	Reference pressure
Γ_d	Dry adiabatic lapse rate
Γ	Environmental lapse rate
T_v	Virtual temperature
θv	Virtual potential temperature
q	Specific humidity
$\bar{q}$	Watervapour mixing ratio
r	Mixing ratio
$\bar{C}$	Pollutant concentration
z_i	Inversion altitude
U_t	Transport wind speed
I	Intensity of transmitted light
Io	Intensity of incident light
Cs	Speed of sound
R_d	Universal gas constant for dry air
d	Path length
γ_d	Specific heat ratio of dry air
V_d	Velocity component of sound pulse between transducers

σ	Standard deviation
μ	Mean
S	Shear production
B	Buoyancy production
D	Dissipation of energy
Tr	Energy transported with turbulent flow
m	Metre
s	Second
mb	Millibar
Hz	Hertz
ng	Nanogram
µg	Microgram
σ_{air}	Mass absorption cross-section
R	Pearson's correlation coefficient
X	Independent variable
Y	Dependent variable
$\overline{X}$	Mean of independent variable
$\overline{Y}$	Mean of dependent variable
b	Slope of the regression line
a	y-intercept

CHAPTER 1

INTRODUCTION

The Earth's atmosphere is a thin life-giving gaseous blanket which is comprised of many gases. Numerous physical processes occurs in the earth's atmosphere, which drive the temperature and wind speed patterns. According to the variations in temperature with respect to the height, the atmosphere is divided into different layers. The lowest layer of the atmosphere is called as the troposphere which is capped by the tropopause. The troposphere extends to an average altitude of about 16 km from the ground in the tropics to about 9 km in the polar region (Ahrens, 1998).

Atmospheric boundary layer (ABL) is defined as that part of the troposphere that is influenced directly by the earth's surface and having a response to the surface forcing with a timescale of an hour or less (Stull, 1988). The main elements of surface forcing present in the boundary layer are frictional drag, evaporation and transpiration, heat transfer, emission of pollutants and terrain-induced flow modification etc. The remaining air in the troposphere is called as the free atmosphere (FA). One of the important transportation processes that occurs in the boundary layer is turbulence, due to which the vertical transport of heat, momentum, moisture, energy, and pollutants takes place (Stull, 1988). Turbulence is characterized by random three-dimensional irregular fluctuations around some mean flows, transporting mass/energy/momentum across it (Arya, 2005). Thus, ABL is region responsible for controlling or modulating the transfer of surface energy/ forcing to the free atmosphere and plays an important role in Earth's energy budget.

ABL depth (or the height of the top of the ABL above ground) shows high spatio-temporal variability depending on the terrain, topography, incoming solar radiation, seasons, surface roughness etc. Winds in this layer can be divided as mean wind, turbulence and the waves (Stull, 1988). The concentration of the pollutants in the ABL is built up by the low winds and the weak vertical mixing. Due to the

absence of strong solar radiation during the monsoon and the winter periods the depth of the ABL seems to be low during these times. The diurnal variation of temperature is a distinct characteristic of the boundary layer as it is not much prominent in the FA. ABL attains its maximum depth in the afternoon hours. For air quality studies, the so-called ABL is of primary importance. As most of the pollutants are emitted into this layer, gets transported horizontally and vertically, the structure of the ABL has important implications for air quality. Therefore information on the vertical structure and the characteristics of the ABL are necessary for air quality studies.

The structure of the ABL can be divided into different sub layers like the surface layer, mixing layer, entrainment zone, residual layer and the nocturnal boundary layer. Surface layer (SL) (shown in light blue colour in Fig. 1) is the lower most part of the atmosphere and is having a direct influence on the daily activities occurring at the surface of the earth (Fig. 1). The thickness of this layer is about 10% ABL (Stull, 1988). Throughout the SL, the meteorological variables like the wind speed, temperature and humidity change with height. Wind shear plays a dominant role in the SL. For the interpretation of the local and global climatology the role of the atmospheric surface layer in the energy exchange processes is essential (Geenaert, 2003). After the sun rise, the surface gets heated due to the interaction of solar radiation with it, which results in the rising of thermals along with lifting up the previous night's inversion layer. As the day progresses, more and more thermals formed, thereby increasing the ABL depth which results in an increased volume for the mixing of the heat, moisture, momentum and also air pollutants in the vertical. This layer is called as the mixing layer (ML) shown in light green colour in Fig.1. The mixing processes happen due to the absorption of solar radiation by the surface which leads to the rising thermals (thermal turbulence) and due to the in homogeneities introduced by clouds, aerosols, terrain features etc., and are distributed across the atmosphere partly by the wind shear (mechanical turbulence). Therefore mixing layer height (MLH) serves as a significant parameter for air quality studies (Holzworth, 1967; Stull, 1988; Mues *et al.*, 2017). It can also be called as the convective boundary layer (CBL). The mixing layer and free

atmosphere is separated by entrainment zone (EZ) (shown in yellow colour in Fig. 1). It acts as a lid above the ML. Solar radiation is absorbed by the surface in a non-uniform manner. As a result, at some places, the thermals will rise whereas at some other places there will be subsidence. Therefore a combination of updrafts and downdrafts can be observed. If the convective plumes are highly strong they may escape from the ML to FA at some places while at places where subsidence occurs, the air from FA may entrain into the ML. In the presence of strong convection EZ becomes deeper. By late afternoon, turbulence starts decaying due to the decrease in surface temperature happening due to the reduction in surface-reaching shortwave solar radiation. Thus, EZ gets replaced by capping inversion (CI) (shown in grey colour in Fig. 1). The radiative cooling of the surface and the reduction in thermals lead to the formation of the residual layer (RL) (shown in pink colour in Fig. 1) which obtains its name as its concentration variables are the same as those in the ML. The lower portion of the RL in contact with the ground gets modified into a stable shallower layer as the night progresses called as the nocturnal boundary layer (NBL) (shown in violet colour above the surface layer in Fig. 1). The inversion builds up with time throughout the night partially due to the decrease in surface temperature and somewhat due to the mixing happening due to night-time wind shear induced mixing.

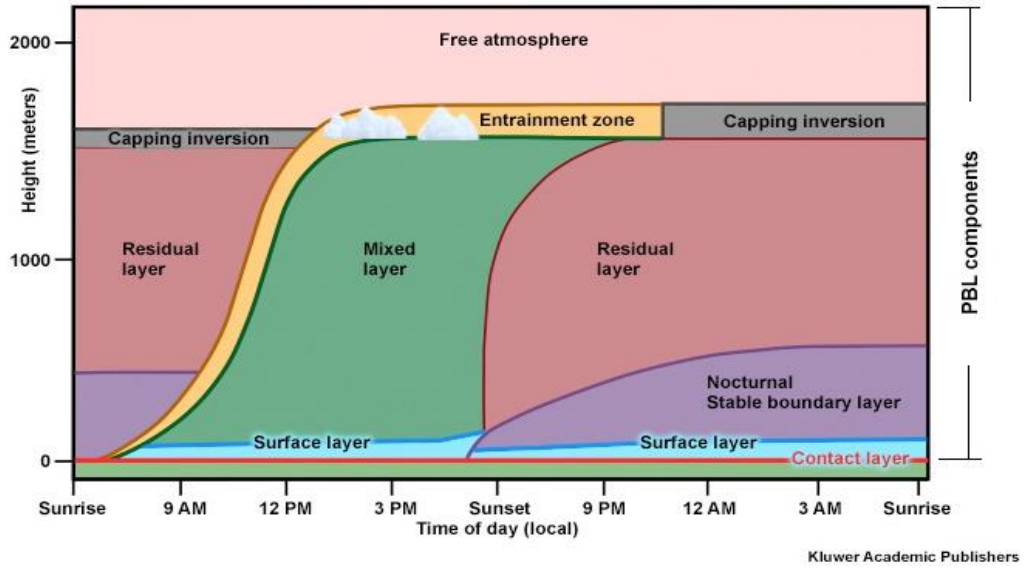

Fig. 1. Diurnal evolution of ABL, during fair weather conditions (Stull, 1988).

Globally, adverse air quality is a serious environmental risk which arises from the emissions out of the rapid industrialization associated with the increased economic growth. Apart from the several gaseous components present in the Earth's atmosphere, it also contains numerous tiny suspended solid or liquid particles. These suspended solid or liquid particles in the atmosphere, that affects air quality, weather and climate through different mechanisms are called as the atmospheric aerosols. Since sources of aerosols are present within the boundary layer, aerosols are most concentrated within this lowest atmospheric layer.

The word aerosol was coined about 100 years ago (during 1920's) as an analog to the term hydrosol, which refers to a stable liquid suspension of solid particles (Hinds, 1999). Size of aerosols ranges from a few nanometers (nm) to hundreds of micrometers in diameter (Satheesh *et al.*, 2004). Depending on the source of production, they can be of natural (e.g. sea-spray, dust storms, volcanic eruptions etc.) as well as anthropogenic origin (e.g. burning of fossil fuels, industrial emissions, transportation etc.). Whether natural or anthropogenic, aerosols are produced mainly by the process of mechanical disintegration occurring over land (lifting up of soil and sand particles by the effect of wind) and ocean (sea spray droplets due to wind) and by gas to particle conversion process (condensation

or nucleation of low volatile gases) occurring in the atmosphere (Prospero *et al.*, 1983; Satheesh *et al.*, 2004). The particles formed by mechanical disintegration process (primary aerosols) are generally larger in size as compared to that of those formed by gas to particle conversion (secondary aerosols) (Satheesh, 2002).

A broad classification of aerosols, depending on its size, can be made as the nucleation mode or Aitken mode (radius 0.001 to 0.1 μm) which has a dominant role in atmospheric electricity, the accumulation mode (radius 0.1 to 1 μm) which has a major influence on the radiation budget, and the coarse mode (radius > 1 μm) particles which can act as cloud condensation nuclei (CCN). Nucleation of volatile gases lead to the formation of nucleation mode aerosols through the gas to particle conversion (Satheesh, 2002). The accumulation mode particles are formed by the coagulation of the smaller particles to form a bigger particle and the coarse mode particles are formed from mechanical processes like the direct action of the wind on aerosols.

Once airborne, different processes transform the size and composition of the aerosols such as coagulation (collision and coalescence with other aerosol particles), condensation of vapours on aerosols, and by chemical reactions occurring in the atmosphere (Satheesh *et al.*, 2004). The overall lifetime of aerosols depends on the properties of the aerosols, thermodynamic and meteorological characteristics of the area, and different layers in the atmosphere.

Major removal processes of atmospheric aerosols include dry deposition or sedimentation (gravitational settling) and wet removal (wash out) (Satheesh *et al.*, 2004). Dry deposition represents the deposition of aerosols to the earth's surface under the influence of gravity. Larger aerosol (coarse mode) particles get deposited at the earth's surface quickly while the smaller particles (accumulation and Aitken mode) remain in the atmosphere for longer time periods. The scavenging of aerosols from the atmosphere due to the effects of rain drops or any other precipitation events is called as the wash out or the wet deposition. Aitken and accumulation mode particles (radius < 1 μm) are removed by the wet deposition processes. It involves two major mechanisms like, in-cloud scavenging and impaction scavenging. In

nucleation scavenging, most of the water vapour present in the atmosphere condense on aerosol particles and form droplets. These droplets increase in size due to coagulation resulting in precipitation. Impaction scavenging occurs below the cloud. Aerosol particles are removed along with the rainfall or any other precipitation events.

Based on the composition, aerosols, in general, consist of sulfates, nitrates, sea salt and non-sea salt particles, mineral dust, organic and carbonaceous compounds. Most of the aerosol particles including sulfates cool the climate system (Bond *et al.*, 2013). Carbonaceous compounds refers to the aerosol black carbon (BC) particles which are the absorbing component of soot and often defined using elemental carbon and some defined organics (Ramanathan and Carmichael, 2008) and these constitutes the most important aerosol types (Satheesh *et al.*, 2004). BC particles are produced in large amounts as a combustion product from fossil fuel burning, cooking with bio fuels such as crop residue, dung, and wood etc. (Jacobson, 2001). Among the aerosol particles, those with serious implication on local as well as global temperature change are the BC particles. According to Intergovernmental Panel on Climate Change (IPCC), BC particles constitute the third most important anthropogenic warming agent after carbon dioxide and methane (IPCC, 2007). It not only absorbs a significant portion of the solar radiation (Bond *et al.*, 2013), but also decreases the net albedo of polar ice caps and glaciers (Ramanathan and Carmichael, 2008), which ultimately results in the warming and melting of the ice. BC particles are removed from the atmosphere by wet deposition process which interferes with the vertical distribution of the particles and limits its residence time to one week (Ramanathan and Carmichael, 2008; Bond *et al.*, 2013).

In order to quantify the large uncertainties persisting in the global climate predictions, understanding of the formation, physical, chemical, and optical properties, and the transformation of the aerosols are of crucial importance (Prospero *et al.*, 1983). The optical properties of aerosols include scattering, absorption, aerosol optical depth, single scattering albedo, asymmetry parameter etc. (Boucher *et al.*, 2013). Scattering refers to the process by which particles

(scatterer) continuously abstracts electromagnetic (EM) radiation incident on it and re-emits it into a solid angle centred around the particle (Satheesh *et al.*, 2004). Scattering can be elastic or inelastic. In elastic scattering, energy is conserved between scattered and incident radiation. Hence internal energy of the scatterer remains constant. In inelastic scattering a part of the incident radiation is used to produce changes in the internal energy of the scatterer. Depending on the wavelength of incident radiation and the size of scatterer, elastic scattering can roughly be divided into Rayleigh (scatterer size < $1/10^{th}$ the wavelength of incident radiation) and Mie scattering (scatterer size > ~$1/10^{th}$ the wavelength of incident radiation) (Satheesh, 2002). The intensity of Rayleigh scattering varies inversely with the fourth the power of wavelength and directly with the scatterer volume. Equal intensities are scattered in both forward and backward direction. Hence, it can be said that the angular distribution is symmetric in Rayleigh scattering. Atmospheric aerosols exhibit Mie scattering. Scattering pattern in this case is more complex as the particle size is larger compared to the wavelength of incident radiation (Platt *et al.*, 2007). The angular distribution is assymetric with forward lobes dominating.

Change in radiation flux caused by the aerosols is called as the aerosol radiative forcing (RF) (Satheesh *et al.*, 2004). RF from the aerosol differs from that of the greenhouse gases in several ways (Charlson *et al*., 1992). The most important parameters which define the radiative properties of aerosols are the columnar loading of aerosols, represented through the aerosol optical depth (AOD) and the ratio of scattering to extinction (combined effect of scattering and absorption), represented through the single scattering albedo (SSA). Quantifying the concentration and optical properties of BC aerosols, their vertical distribution, and temporal variations are hence essential in both air quality and climate change studies (Satheesh *et al.*, 2004).

BC aerosols absorb the solar radiation and ultimately results in global warming (Ramanathan and Carmichael, 2008). Radiative effects of aerosols can be direct or indirect. Direct radiative effects can be defined as the scattering or

absorption of solar radiation by aerosol particles. This affects the climate system by changing the reflection (albedo) of planet. Indirect radiative effects correspond to the ability of aerosols to act as CCN and ice nuclei and thereby affecting the cloud radiative properties. When more aerosols enters into the clouds the effective droplet size gets reduced (this increases the cloud albedo) thereby inhibiting precipitation (Satheesh *et al.*, 2004; Boucher *et al.*, 2013). This increases the lifetime of the clouds. Effective droplet size influences the radiative properties of clouds.

BC contributes large positive atmospheric forcing. Direct RF from BC is estimated to be +0.4 W m^{-2} (+0.05 to +0.8) (Boucher *et al.*, 2013) which is very large compared to other aerosol particles. At the end of 21st century (2081-2100) the global surface temperature change is likely to exceed 1.5 °C for representative concentration pathway (RCP) 4.5, 6, and 8.5 (high confidence) compared to that of 1850-1900 (IPCC, 2014). BC also play a major role in deteriorating the air quality and visibility. They can also have serious impacts on the health by enhancing respiratory cardiovascular, infectious and allergic diseases (Pöschl, 2005). Ultrafine particles (<100 nm) are small enough to penetrate the membranes of respiratory tract and gets transported along with the blood (Nemmar *et al.*, 2002). BC particles are also reported to be carcinogenic in humans (Afroz *et al.*, 2003).

The weather conditions play a significant role in air pollution episodes by transportation of the pollutants. So, it can be said that the air quality is strongly dependent on weather parameters, and therefore are sensitive to climate change (Jacob and Winner, 2009). The ABL characteristics may change due to the synoptic conditions, seasons, surface friction due to vegetation, topography, soil moisture conditions, agricultural practices etc. (Stull, 1988; Sandeep *et al.*, 2014). Analysing the variation of fundamental variables in the ABL and causes of such variations are crucial in air quality and meteorological studies. BC aerosols being chemically inert in the atmosphere can be used as a tracer for air pollution. The ABL characteristics are governed mainly by the down welling solar radiation. BC absorbs the solar radiation and decreases the amount of solar radiation reaching the ground and hence interferes with the stability of ABL. In this thesis, the temporal variation and the

association of BC concentration with ABL dynamics and dispersion are studied to address the role of ABL dynamics in controlling the near-surface aerosol concentration and thereby the air quality. Chapter 2 presents a comprehensive review on aerosols and ABL. Experimental site description, observational data and instrumentation, and the methodology followed are detailed in Chapter 3. Results and discussion are given in chapter 4. This thesis is concluded by chapter 5.

CHAPTER 2

REVIEW OF LITERATURE

2.1 ABL processes

2.1.1 Turbulence

The atmospheric turbulence (shown schematically in Fig. 2) is the random, chaotic motion of the air within the atmosphere. Or else it can be described as the gustiness superimposed on the mean wind (Stull, 1988). Some of the general characteristics of turbulence include randomness or irregularity, three dimensional and rotational flow, diffusivity or the ability to mix property (like momentum, mass and heat), and dissipativeness (constant energy supply is needed to maintain turbulent motion, otherwise it decays) (Arya, 2001). The mixing ability of ABL turbulence determines the air quality of regions to a large extend. This random motion consists of irregular swirls of different sized eddies superimposed on each other. Eddies in a turbulent flow are those whirl like complex three dimensional structures which have a very wide size range (for ABL, typical eddy size range is of 10^{-3} to 10^{3} m) (Arya, 2001). Various types of turbulence present in the atmosphere are the clear air turbulence, mechanical turbulence, frontal turbulence, convective turbulence etc. The major sources of turbulence within the atmosphere are the wind shear and the convection. The intensity of atmospheric turbulence can be represented by turbulence kinetic energy per unit mass (TKE) (Arya, 2001). TKE is given by,

$$d(TKE)/dt = S + B - D + T_r \quad (1)$$

From eq. 1. it is clear that the shear production (S) and buoyancy production (B) represents two generating mechanisms of turbulence, and also there is continuous dissipation (D) of energy due to viscosity (which means the resistance to flow or friction) and transport (T_r) of energy associated with the turbulent flows. Therefore, in order to maintain the turbulent flow either shear or buoyancy or both is necessary. Both shear and buoyancy contribute to the turbulence generated in the day time

unstable ABL, while in the stable NBL, turbulence is generated by wind shear. The interaction of solar radiation with the ground heats the air above and thus results in the rising of heated air due to buoyancy. Thus, the eddies and buoyancy production are directly related since they consist mainly of heated air at the surface and these eddies are known as the thermals or plumes (Nieuwstadt and Duynkerke, 1996). In addition to the shear and buoyancy, any inhomogeneity present in the atmosphere may also leads to the development of turbulence. The variations in the wind flows may be occurred due to the presence of the surface features like buildings, forests, mountains, valleys etc. The most common approach for analysing the waves and turbulent motion is to split the variables like the temperature and the wind into the mean and the perturbation part. Reynolds decomposition can be used to manifest any variable in turbulent flow as a sum of its mean and turbulent fluctuation (Arya, 2005) which can be represented as,

$$u(t) = \bar{u} + \acute{u} \tag{2}$$

$$v(t) = \bar{v} + \acute{v} \tag{3}$$

in which the left hand side represents instantaneous variable and right hand side represents the sum of mean (denoted by a tilde) and turbulent part (denoted by an apostrophe).

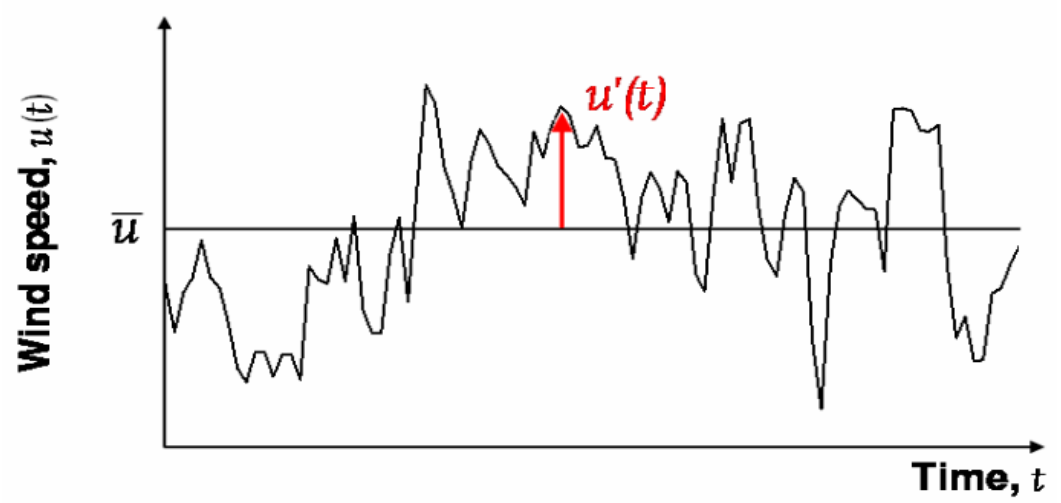

Fig. 2. Wind speed variation with time. u(t) is the instantaneous wind speed, ū is the mean wind speed, u' is the turbulent fluctuation and t is the time (Wood, 2007).

2.1.1.1 Wind speed spectrum

While analysing the wind speed spectrum (shown in Fig. 3) two large peaks with a pronounced gap in between them can be observed. The peak to the left of the gap represents the synoptic scales having a larger time period (lower frequency) and that to the right of the gap represents the micro scale or turbulent scale, flows having a higher time period (higher frequency). The gap separating the micro scale and the synoptic scale peaks is known as the spectral gap, with the centre of the gap having roughly an hour time period, which is the reason why the one hour time frame is often used while defining the atmospheric boundary layer.

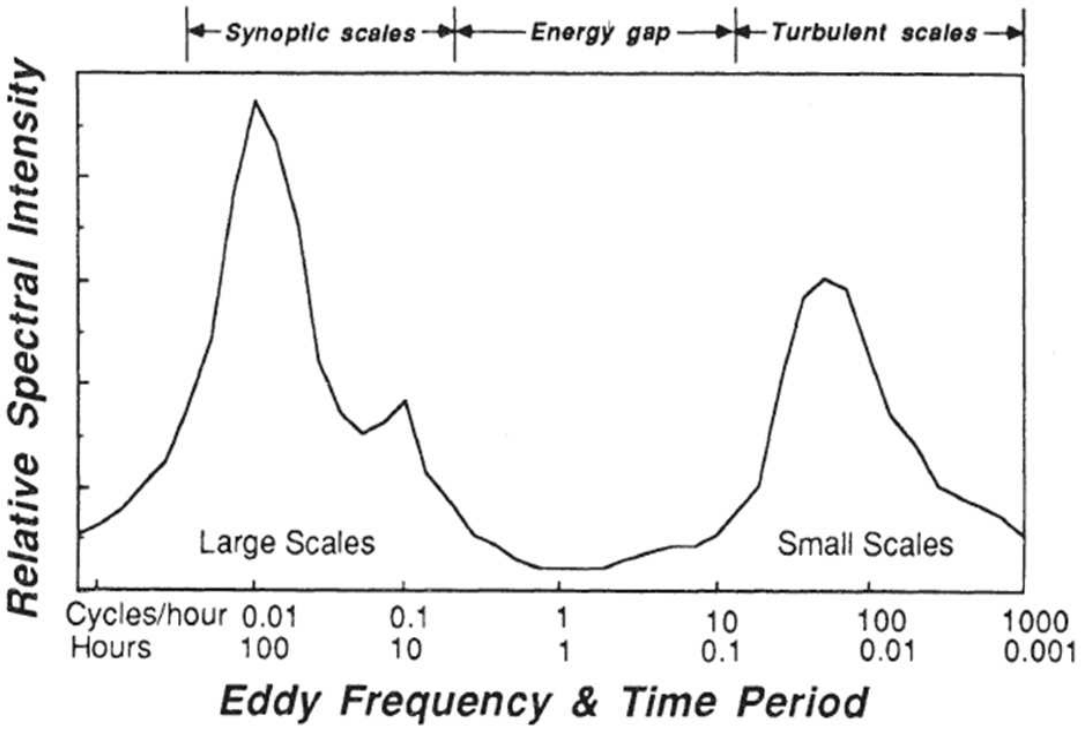

Fig. 3. Wind speed spectrum (Stull, 1988).

2.1.1.2 Energy cascade hypothesis

The energy cascade process was put forward by Lewis Richardson in 1922. This provides information on the atmospheric turbulence processes and the down scale energy transfer processes. Energy distribution in an atmospheric system is non uniform. This can be described using an energy spectrum. It consists of three major spectral regions like the energy containing range (which contains almost all of the TKE produced as a result of shear and buoyancy), inertial sub range (where there is no net gain or loss of energy but gets transferred to smaller scales), and the dissipation range (where the TKE is dissipated to internal energy through viscosity). And the energy cascade process explains the energy transfer mechanism from large eddies to smaller eddies which also involves intermediate eddies. Large eddies which are mainly produced by the mean flow convection and shear contains almost all of the energy. Eddies grow larger and larger until the characteristic length scale of mean flow. When these larger eddies becomes highly unstable they breaks down to smaller and smaller scales. Almost all of this energy gets dissipated by small

eddies through viscosity. The smaller eddies are produced by the break down of larger eddies and the energy transfer occurs during the break down process. The energy cascade process is well-documented in several literatures (Kaimal and Finnigan, 1994; Arya, 2001).

2.1.2 Atmospheric stability

Incoming solar radiation leads to the heating up of the surface and this in turn heats up the near surface air parcels which leads to the rising up of the air parcels up to an altitude until it experience thermal equilibrium with the surrounding air. While when the air parcels near to the surface are cooler than the surrounding air, the convective lifting of the air parcels are inhibited. An air parcel rises up when its density is less than that of the surrounding air at the same pressure. Thus the buoyant force acting on the air parcels describes the atmospheric stability. The buoyancy can be positive, negative and zero. When the temperature of the air parcel is higher than the surrounding air then the parcel will be displaced upwards from its position. Such a condition is called as positive buoyancy. And an air parcel is said to be negatively buoyant when the air parcel have a lower temperature than the surrounding air and thereby the parcel will be displaced downwards from its position. When there is no difference between the temperature of the air parcel and the surrounding air the air parcel remains in its position itself and this condition is called as the zero buoyancy. Certain characteristics of the atmosphere like the passive scalar behaviour is significant in terms of combustion, pollutant mixing etc. Passive scalar represents a diffusive contaminant in atmospheric flow with no thermodynamic effects (like buoyancy) on the atmospheric flow (Warhaft, 2000). Therefore analysis of the temperature of air parcels with respect to the surroundings helps in estimating the stability of the atmosphere. In order to consider the atmospheric stability, the concept of potential temperature is often introduced in this context. The atmospheric stability can be well measured by the use of potential temperature. Potential temperature can be defined as the temperature an air parcel with absolute temperature T and pressure P would have if brought adiabatically to the pressure at 1000 mb (millibar) level. T and θ are equal at 1000 mb pressure by

definition. Standardization of pressure of air parcels will enable to compare the parcels existing at different temperatures. To the first order, potential temperature can be written as,

$$\theta = T + (g/C_p)\,\Delta z, \tag{4}$$

where R is the gas constant for dry air (287 J kg^{-1} K^{-1}), C_p is the specific heat at constant pressure (1004 kJ kg^{-1} K^{-1}), T and P represent the temperature and pressure respectively at an altitude 'z' and P_0 represents the reference pressure to which the air parcel is brought down adiabatically.

The stability of atmosphere can be represented by θ though lapse rate given by,

$$\frac{d\theta}{dz} = \frac{\theta}{T}(\Gamma_d - \Gamma) \tag{5}$$

where Γ represents the environmental lapse rate (ELR) (it is the actual temperature existing at a given location as sensed by a thermometer at a fixed height) and Γ_d represents the dry adiabatic lapse rate (DALR) (the rate of temperature change of unsaturated air parcel with height, ie., the rate at which dry air parcel cools when it moves upwards through the atmosphere and the rate at which it warms as it moves towards the ground) (Oke, 1978).

Under the negatively buoyant condition the surrounding temperature of the parcel decreases with height but will be slower than displaced parcels temperature. That is $\Gamma < \Gamma_d$. Therefore in this case $\frac{d\theta}{dz} > 0$. This implies the stable condition.

Under positively buoyant condition the surrounding temperature decreases with height faster than the displaced parcel's temperature, so $\Gamma > \Gamma_d$ resulting in $\frac{d\theta}{dz} < 0$. And the condition is called unstable condition.

When the displaced parcels temperature and the surrounding temperature decreases at the same rate with respect to the height, $\Gamma = \Gamma_d$. Therefore $\frac{d\theta}{dz} = 0$ and this denotes the neutral condition. Therefore it can be concluded that the atmospheric stability can be well explained by the potential temperature profiles.

In the presence of sufficient moisture the contribution of the moisture to the air density is included by defining virtual potential temperature. The virtual potential temperature,

$$\theta v = \frac{\theta}{t} \times T_v \quad (6)$$

where T_v is the virtual temperature which is defined as the temperature that a dry air parcel should attain to have the same density of moist air parcel at the same pressure. The virtual temperature T_v is related to the dry air temperature by the equation,

$$T_v = T\,(1 + 0.61q) \quad (7)$$

where q is the specific humidity, and T is the absolute temperature.

2.1.3 Vertical profile of mean variables in convective boundary layer and stable boundary layer

Fig. 4. shows the variation of the virtual potential temperature (θ_v), wind speed ($\overline{U}$), water vapour mixing ratio ($\overline{q}$) and pollutant concentration ($\overline{C}$) in the convective boundary layer. Mixing ratio is defined as the ratio of amount (mass) of substance in a given volume to total amount (mass) of all constituents in that volume (Seinfeld and Pandis, 2016). It is observed that these parameters exhibit a different pattern in different layers of the ABL depending on the physical characteristics of those layers. In the lowest few metres of the ABL, where super-adiabatic conditions prevail due to the enhanced heat transfer between the underlying surface, gradation in virtual θ_v, $\overline{U}$, $\overline{q}$, and $\overline{C}$ can be observed. Due to the presence of strong convective mixing within the ML, almost all the vertical variations in the above parameters will be smoothed out. $\overline{C}$, and $\overline{q}$ are high near the surface and decreases as the height increases. $\overline{U}$ increases with altitude within the SL due to the decrease in the frictional drag. At the inversion layer, as entrainment of air between the FA and ML occurs, θ_v, and $\overline{U}$ increase in the inversion layer.

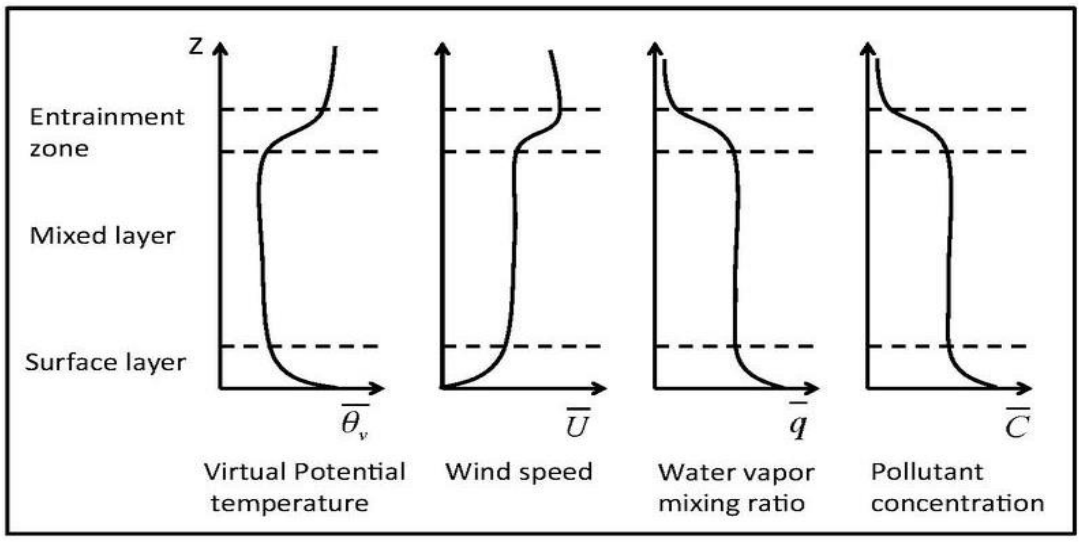

Fig. 4. Profiles of virtual potential temperature (θ_v), wind speed ($\overline{U}$), Water vapour mixing ratio ($\overline{q}$), pollutant concentration ($\overline{C}$) within the convective boundary layer (Stull, 1988).

The inversion layer deepens with time as the cooling continues (shown in Fig. 5). The potential temperature follows a neutral profile that is an adiabatic cooling with the altitude. As the evapotranspiration is lowest during the night the humidity mixing ratio (r) is lowest at the surface layer. As there are few sinks and sources for water vapour, values of humidity mixing ratio throughout the residual layer remains as that of the previous day. There is little source for water vapour above the capping inversion thus 'r' reduces very sharply. As the free convention ceases after the sunset, vertical transfer of horizontal momentum by buoyant plumes and thus the frictional forces are experienced by a shallow layer.

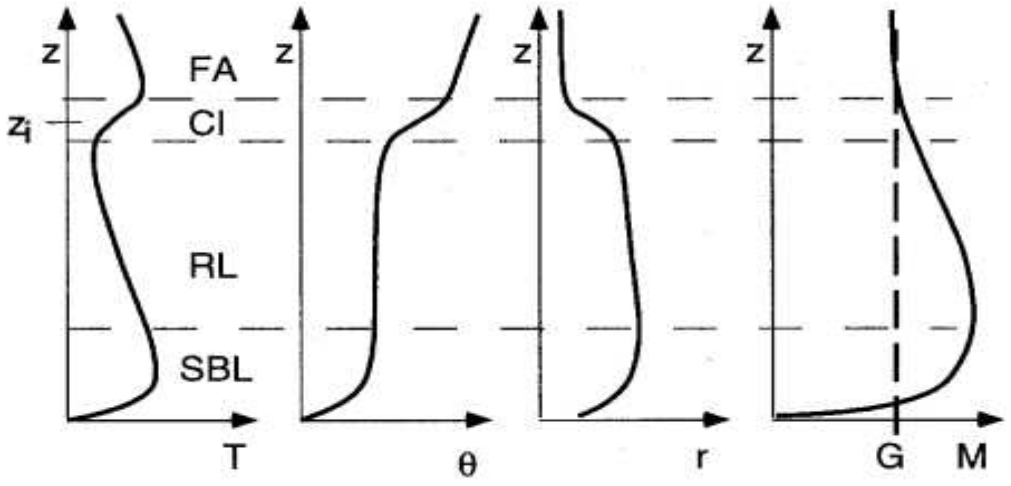

Fig. 5. Typical nocturnal profiles of temperature(T), potential temperature(θ), humidity mixing ratio(r), and horizontal wind speed(M) in the nocturnal boundary layer. G denotes the geostrophic wind. The boundaries between the layers are marked by the dashed lines. SBL denotes the stable boundary layer, RL implies the residual layer, CI represents the capping inversion, and FA denotes the free atmosphere and altitude is z, inversion altitude is z_i (Stull, 1997).

2.1.4 Spatial pattern of ABL height

ABL height varies over different geographical locations spatio-temporally. It depends on the terrain, topography, convection available at the surface, synoptic weather patterns and the existing land surface conditions (Stull, 1988; Patil *et al.,* 2013). Santanello *et al*. (2005) reported that the stability conditions and the soil moisture content account for 76% of variance in the planetary boundary layer (PBL) height. Patil *et al.* (2013) found that the PBL height is gradually increasing from south to north in the Indian subcontinent and largest PBL height is observed in the north-western part of India during the monsoon season. It is also observed that due to the intense solar heating during the pre-monsoon season, larger PBL heights (≈1800 m) are observed in most regions of the Indian subcontinent. Sathyanadh *et al*. (2007) showed that the Boundary layer height decreases during the monsoon season as a result of enhanced entrainment and also reported the influence of evaporative fraction and net radiation on the evolution of PBL. The MLH over the

coastal regions are influenced by the sea and land breeze circulations and also results in the formation of thermal internal boundary layer (Nair *et al.*, 2011).

Several experiments to investigate the oceanic ABL were also carried out on a global scale. In past few decades several ship borne experiments were executed in order to estimate the marine atmospheric boundary layer (MABL) like Atlantic Trade wind Experiment (ATEX), GARP Atlantic Tropical Experiment (GATE), First GARP Global Experiment (FGGE), Tropical Ocean Global Atmosphere (TOGA) which provided the thermodynamic structure of the MABL over the Pacific and Atlantic oceans. The Indo Soviet Monsoon Experiment (ISMEX-73), MONSOON 77 and the Monsoon Experiment (MONEX 79) were conducted to characterise the MABL over the Bay of Bengal (BoB) and Arabian sea (AS) (Alappattu and Kunhikrishnan, 2010). The experimental observations conducted by Alappattu and Kunhikrishnan, (2010) reported that the ABL height over the BoB corresponds to 400-1200 m period and about 375-1200 m over the AS during the pre-monsoon.

2.1.5 Importance of atmospheric boundary layer studies

Significance of ABL lies in several domains like climate, weather forecasting, agricultural meteorology, hydrology, air pollution and urban meteorology etc. Dispersal of pollutants and smog depends highly on the meteorological conditions, ABL dynamics, and long-range transport processes. Investigations on meteorological parameters and ABL height are inevitable in studies related to the assessment of air pollution and wind power (Xiang *et al.*, 2019). The role of ABL dynamics in controlling the near-surface pollutant concentration is well discussed in many studies (Babu and Moorthy, 2002; Nair *et al.*, 2007; Aruna *et al.*, 2013; Begam *et al.*, 2016). The ABL height is the maximum available volume for intense mixing and thus influences the dispersion of pollutants. The exchange of heat, momentum, moisture and mass between the surface and the lower atmosphere regulates major physical processes occurring in the atmosphere and are strongly dependent on the ABL dynamics. A primary requirement in climate modelling is hence to obtain better parametrization for these processes, which can be ensured by accurate observations of ABL and the exchange

processes happening within it. ABL height is a significant parameter in weather and climate models (Mahalakshmi *et al*., 2011). ABL influence the dynamics of the atmospheric processes.

2.1.6 Aerosols and boundary layer interactions

A large volume of aerosols resides within the ABL and a strong interaction takes place between them. ABL is innately connected to the air pollution (Yu *et al.,* 2002). Even if the rate of emission remains the same, the interactions between the aerosols and the ABL can intensify the air pollution. The aerosols present in the ABL scatter/absorb the downwelling solar radiation and thereby reduce the amount of radiation reaching the surface. As a result, surface heating and thereby the convective turbulence reduces, leading to a reduction in the mixed layer height. This leads to increased moisture (density) in the ABL which promotes the growth of the aerosol particles within the ABL. Due to a large proportion of aerosol particles residing within the ABL, and as strong feedbacks exist between them, it can be concluded that ABL is intrinsically connected to air pollution episodes (Li *et al.*, 2017). Modelling studies done by Yu *et al.* (2002) revealed the significant relationship between aerosols and the ABL height. The boundary layer temperature and humidity control the convective available potential energy. The meteorological and synoptic condition of an area, the weather patterns and the ABL structure and processes have a great influence on the vertical distribution of the aerosol particles (Stull, 1988). It has been observed that a lower aerosol concentration persists near the surface during the summer than in the winter due to the impacts of the summer monsoon precipitation events, the movement of the winds, and the presence of relatively higher boundary layer height which leads to vertical distribution of aerosols to higher levels of the atmosphere.

2.1.6.1 Aerosol Observations

Atmospheric aerosols have been widely studied through various national and international campaigns in order to examine their influence on the global climate system. Some of the international efforts includes the International

Geosphere Biosphere Program (IGBP), Aerosol Characterisation Experiment (ACE), Smoke, Clouds and Radiation Experiments (SCAR), Tropospheric Aerosol Radiative Forcing Observational Experiment (TARFOX), Indian Ocean Experiment (INDOEX) etc. (Satheesh *et al.*, 2004). Prior to 1980's, systematic studies on the aerosols, clouds and radiation budgets were non existing in India except the regular observations of turbidity by India Meteorological Department (IMD) (Satheesh *et al.*, 2004). During the late eighties, Indian Middle Atmosphere Program (IMAP) became operational, and a series of scientific campaign experiments which includes various measurements using the balloons, rockets and satellite measurements were executed. Aerosol characterisation was also carried out using balloon borne and rocket borne payloads which make use of the scattered sunlight to derive the altitudinal profiles of the aerosol extinction. Several ground observatories of Aerosol Radiative Forcing over India NETwork (ARFINET) and Aerosol Robotic Network (AERONET) are spread across India for measuring AOD and Absorption AOD (AAOD). A joint Indo-UK field campaign, South West Asian Aerosol Monsoon Interaction (SWAAMI) aims at the characterization of the aerosol monsoon interactions and their variability across the Indian regions, through a detailed examination of the aerosol physical, chemical and optical properties across India (Pathak *et al*., 2019). Detailed observations of aerosols and clouds are obtained from the satellite remote sensing over the last few decades. The CALIPSO spaceborne lidar (Winkler *et al*., 2010) provides climatology of aerosol extinction coefficients and highlights that over most of the regions the majority of the optically active aerosols are predominant in the lowermost part of the atmosphere of about 1-2 km. Since IPCC AR4 (Assessment Report), many new and improved aerosol data sets have been emerged (Boucher *et al*., 2013). The Integrated Campaign for Aerosols, Gases and Radiation Budget (ICARB) experiments under the Indian Space Research Organisation - Geosphere-Biosphere Program (ISRO-GBP) focussed to address the spatio temporal variation of the atmospheric aerosols and trace gases over the Indian subcontinent and its surrounding oceanic regions.

Several studies have been carried out through out at different geographical locations of India in order to measure the BC mass concentration. It extends from

the coastal regions (Babu and Moorthy, 2002; Aruna *et al.*, 2013) to the Himalayan regions (Pant *et al.*, 2006; Dumka *et al.*, 2010). Studies were also conducted in Island regions (Babu and Moorthy, 2006). Nair *et al*. (2007) reported the BC mass concentration in Indo-Gangetic Plains. Observations were also made from semi-arid regions in southern India (Kumar *et al.*, 2011; Satheesh *et al.*, 2013; Begam *et al.*, 2016; Anand *et al.*, 2020) and also in parts of central India (Kompalli *et al.*, 2014).

2.1.7 Dispersion of pollutants

The air quality over a particular region is intensely effected by the ABL depth and the mean wind of the region. The dispersion of the aerosol concentration is attributed to three major factors such as the source from which they are produced, both the horizontal and vertical redistribution processes in the atmosphere and the removal of the particles from the atmosphere (Satheesh *et al.*, 2013). The air pollution potential of a region is assessed by a parameter called the Ventilation Coefficient (VC). The intensity of the mixing and transport of the pollutants in the ML is obtained from the calculation of the VC (Krishnan and Kunhikrishnan, 2004). Thus, VC is an important parameter of the ABL which represents the ability of the ABL to flush out the pollutant particles and thus has a significant role in the pollutant dispersion and air quality related studies. It is the product of the average speed of transport wind and the MLH in a well-mixed layer. VC is given by the equation,

$$VC = MLH \times U_t \tag{8}$$

where U_t refers to the transport WS in a well-mixed layer.

Several studies conducted in different parts of India reported significant negative correlation between VC and BC (Krishnan and Kunhikrishnan, 2004; Aruna *et al.,* 2013). The dispersion of pollutants in the atmosphere are regulated by atmospheric stability conditions. In order to clearly portray the concept of dispersion, the plume characteristics under different stable and unstable conditions are given in Fig 6.

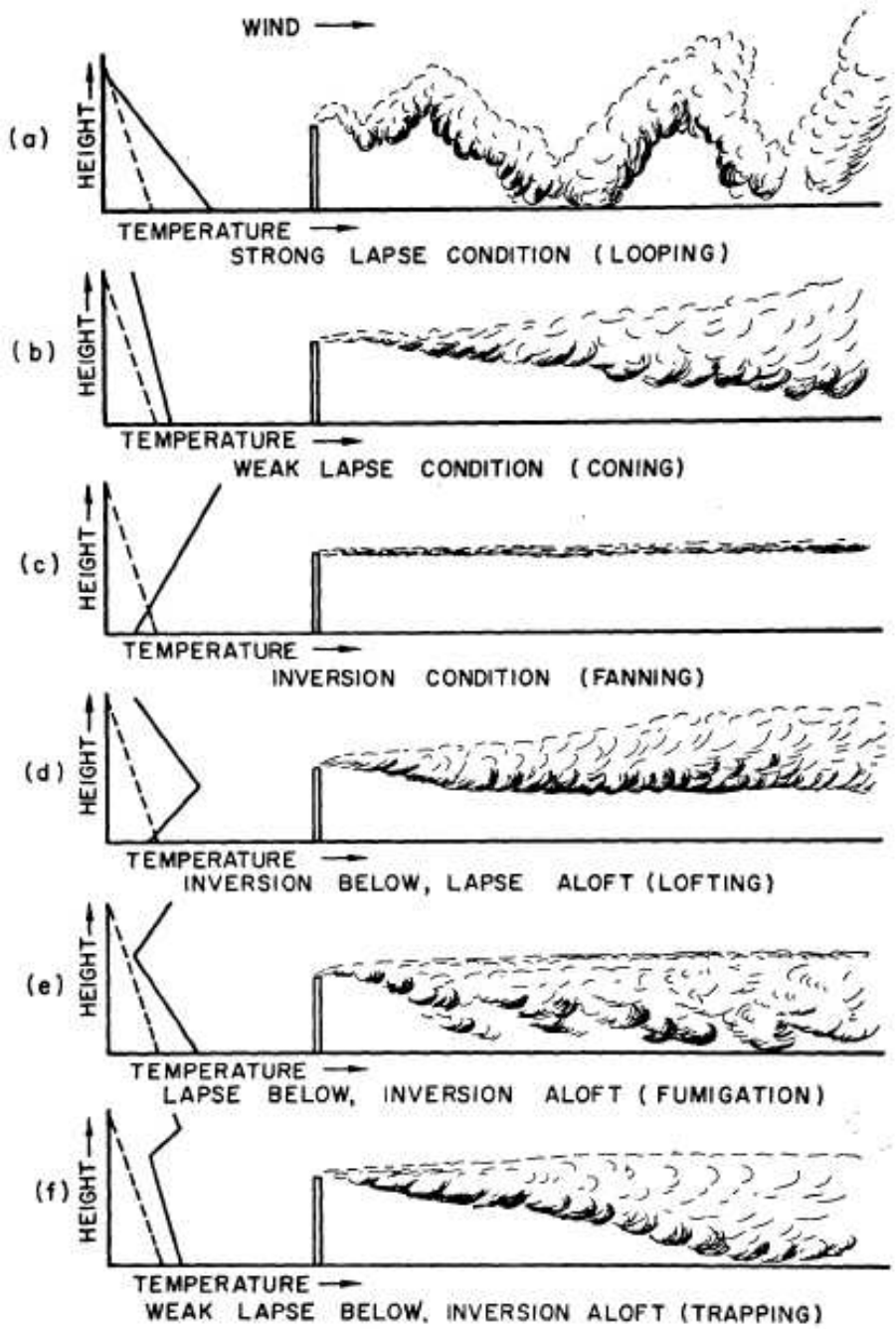

Fig. 6. Characteristic plume behaviour under different stability and instability conditions. The dashed lines represent the DALR and full lines represent the ELR. (a) shows looping behaviour of plumes (strongly unstable condition or super adiabatic), (b) shows coning behaviour of plumes (neutrally stable condition), (c) shows the fanning behaviour (strongly stable condition), (d) shows the lofting behaviour of plumes (weakly stable condition below the stack and super adiabatic

above the stack), (e) shows the fumigation characteristic of plumes (superadiabatic below the opening of stack and stable conditions above the stack), and (f) shows the trapping behaviour of the plumes (weakly unstable below and highly stable above the stack) (Bierly and Hewson, 1962).

In Fig. 6(a) shows the looping behaviour of plumes which exists in a strongly unstable day time condition. Larger eddies transports the plumes in a sinusoidal pattern. This results in bringing undiluted plumes near the ground at very short distance downwind from the stack. Coning behaviour of plumes is shown in Fig. 6(b) which occurs during a cloudy or windy day with neutral stability. In the absence of buoyancy turbulence occurs due to wind shear. So due to weak vertical mixing and slightly stable environment, the suppressed vertical and lateral spreading results in cone like pattern of the plumes. It is seen in the RL of ABL (Stull, 1988). As compared to looping, here the plumes intersect with ground at a larger distance from the downwind of the stack. Under strongly stable atmospheric condition fanning behaviour is shown by the plumes (shown in Fig. 6(c)). Since turbulence is minimum or almost absent under stable conditions, the plumes follow a thin, ribbon like pattern. However due to erratic wind effects it may often forms a V shape which resembles that of a fan when viewed in plane. Due to the lack of vertical transport of the plumes the ground level concentration of pollutants are almost zero. Fig. 6(d) shows the lofting behaviour of the plumes. This is the most favourable plume pattern (Oke, 1978). It is formed during the early evening hours when the radiation inversion starts building up from the ground. Therefore the dispersal of plume towards the ground is blocked but it gets dispersed in the moderately stable layer aloft. Fumigation (shown in Fig. 6(e)) represents the opposite condition of lofting behaviour of plumes. After the sunrise, the ML starts to grow by lifting the previous nights inversion layer. When this turbulent plumes reaches ahead, the pollutants from the stable layer are brought to the near-surface by mixing. This condition exists for a short time-period. Trapping behaviour of the plumes is shown in Fig. 6(f). It refers to the trapping of pollutants in between the surface and the above inversion layer (Stull, 1988).

CHAPTER 3

MATERIALS AND METHODS

3.1 Site description

Continuous, near-real-time measurements of near-surface Black carbon (BC) aerosol concentration has been carried out during March 2018 to February 2019 from the climate observatory located at the second campus of Indian Institute of Science (IISc) at Challakere (14.3° N, 76.6° E, ~580 m amsl) in Karnataka (shown in Fig.7). Challakere represents a semi-arid inland location with scattered short bushes and a near-flat terrain. The annual rainfall is less than 600 mm in the study region. Therefore the region comes under semi-arid climatic zone under Food and Agriculture Organisation (FAO) classification of regions based on annual rainfall (annual rainfall 400-600 mm for semi-arid regions). Previous observations from the region indicated large fraction of sub-micron particles, unexpected for a region with reduced anthropogenic emission (Satheesh *et al*., 2013). The semi-arid terrain (possibility for higher convective lifting time) and the abundance of substantially high concentration of sub-micron aerosols point to Challakere being an ideal choice for studying the air quality. The climatic impacts due to anthropogenic activities can be best studied when the details regarding the near-surface concentration and its vertical redistribution to higher altitudes are known. The redistribution is a manifestation of atmospheric boundary layer (ABL) dynamics, to study which, measurements from a dedicated ABL tower at the study region has been used. Details on the ABL tower, sensors aboard the tower, observational data and its quality check are discussed in this chapter.

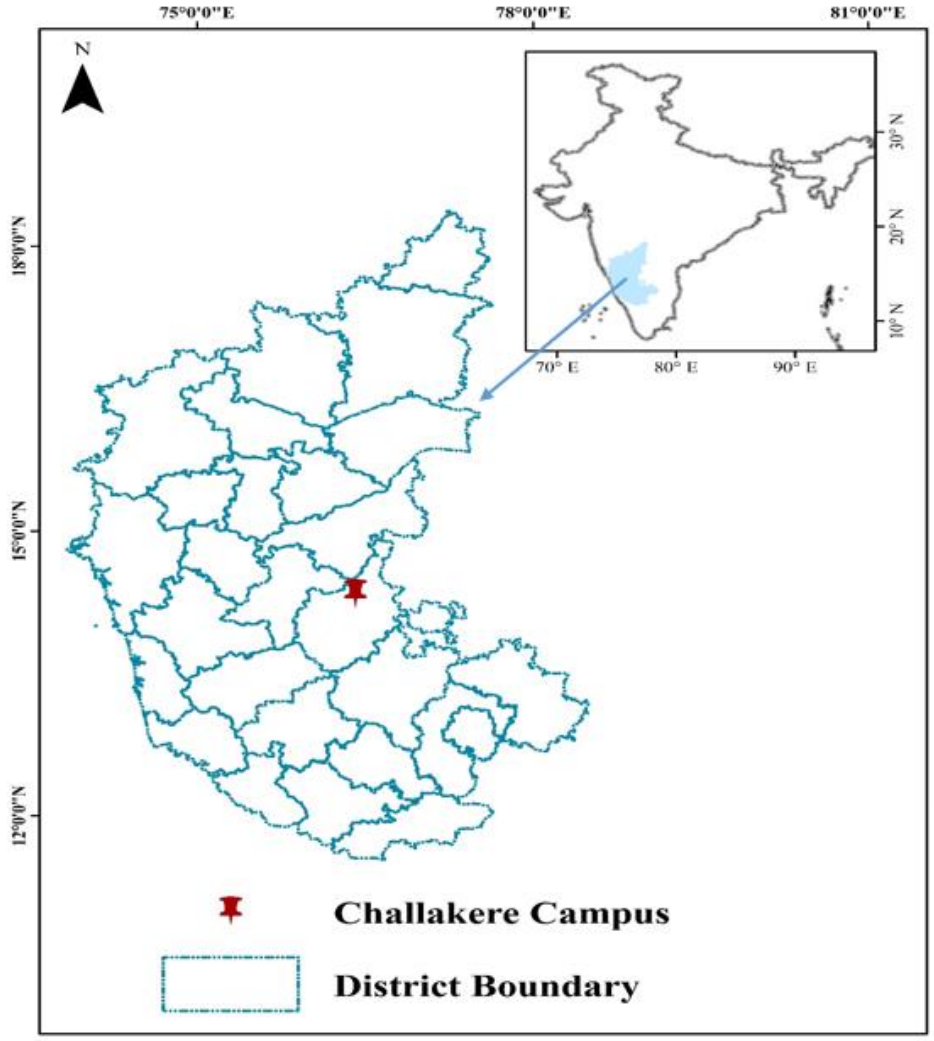

Fig. 7. Location map showing the study region. The IISc Challakere campus is marked by a red pinpoint symbol.

3.2 Observational data

Continuous and collocated near-real time measurements of the BC and ABL parameters carried out from March 2018 to February 2019 have been used in the present study considering three different seasons – winter (December to February, DJF), pre-monsoon summer (March to May, MAM) and post-monsoon (October to November, ON). As cloudy conditions prevailed during the monsoon season (June to September, JJAS) it has not been considered in the present study. BC mass concentration was measured using an Aethalometer (Model AE-33, Magee

Scientific) placed at the top floor of the ~10 m tall laboratory building. Meso/micro meteorological parameters like downwelling solar radiation (SW_{down}), air temperature (AT), relative humidity (RH), wind speed (WS) and wind direction (WD) measured continuously using the slow response sensors (2 m, 4 m, and 16 m) are used in the present study. Clear sky days were identified by the characteristic smooth and inverted U shaped diurnal pattern of down-welling solar radiation. As the ABL dynamics are greatly influenced by the surface reaching short wave solar radiation only clear-sky days were used to study the dispersion of aerosols. Even though this limits the number of available clear sky days, it ensures a well-developed ABL during the day time. The MLH data used in the present study has been calculated by the use of spectral method and was collected from IISc. 30 clear sky days have been used in the present study which includes 10 each for all the three seasons mentioned above.

3.3 Instrumentation

3.3.1 Aethalometer

Near-real-time measurements of BC have been carried out using a seven channel Aethalometer (AE-33, Magee Scientific) shown in Fig. 8. A quartz filter tape is present inside the instrument on which the aerosol particles, continuously aspirated at a flow rate of 5 litres per minutes and with a time base of operation of one minute, are collected after passing through a 1 micron cyclone cut off. There are two spots (collection areas) in the tape, one for collecting the particles and the other one as a reference. BC mass concentration is estimated from the rate of change of the attenuation of light passing through the spot where aerosol particles are collected. The attenuation of light (ATN) derived from the Aethalometer can be represented by the equation:

$$ATN = -100*\ln(I/I_o) \quad (9)$$

where 'I_o' represents the light intensity incident on the filter and 'I' represents the intensity of light transmitted through the loaded filter.

Measurements are made for seven optical wavelengths (Table 1) ranging from ultraviolet to near-infrared in AE-33 and BC mass concentration is derived from the measurement at, 880 nm using a mass absorption efficiency of 7.77 m^2 g^{-1}. 880 nm offers the least absorption from other atmospheric species and hence it offers a better estimate of BC aerosols, as compared to other wavelengths. Other lower wavelengths have higher BC absorption but contains noise from the absorption by other atmospheric species as well and hence will not give the best-estimate of BC. Shadowing and multiple scattering effects are the major sources of uncertainty associated with the estimation of BC from Aethalometer measurements (Weingartner *et al.*, 2003). In AE-33, these are compensated for and hence further corrections are not required (Drinovec *et al.*, 2015). Data from the other channels are used for source apportionment studies and also help in studying the wavelength dependence of the absorption of BC particles.

Table 1. Seven channels in AE-33 and their corresponding mass absorption cross-section

Channel	**Measurement wavelength (nm)**	**Mass absorption cross-section σ_{air} (m^2 g^{-1})**
1	370	18.47
2	470	14.54
3	520	13.14
4	590	11.58
5	660	10.53
6	880	7.77
7	950	7.19

Fig. 8. Photograph of Aethalometer (AE-33, Magee Scientific)

3.3.2 ABL Tower

A 32-m instrumented ABL tower, present in the campus, provides data on various meteorological parameters necessary for the characterisation of the ABL. The tower consists of various sensors (slow and fast response) deployed at five different heights such as 2 m, 4 m, 8 m, 16 m, and 32 m. The meteorological parameters such as solar radiation, AT, RH, WS, WD and Atmospheric-pressure etc. are measured using the sensors aboard the tower. The slow response (1/60 Hz) sensors are mounted at 2 m, 4 m, and 16 m levels and the fast response (20 Hz) sensors at 8 m and 32 m heights. For accurate measurement conditions, the sensors are installed on the tower by considering the orientation and the position of the tower which helps to minimize the disturbance arising from the nearby observatory building. A photograph of the 32 m ABL tower, with the sensor levels marked, is shown in Fig. 9. Details on the make and model of the sensors used in this thesis are shown in Table 2.

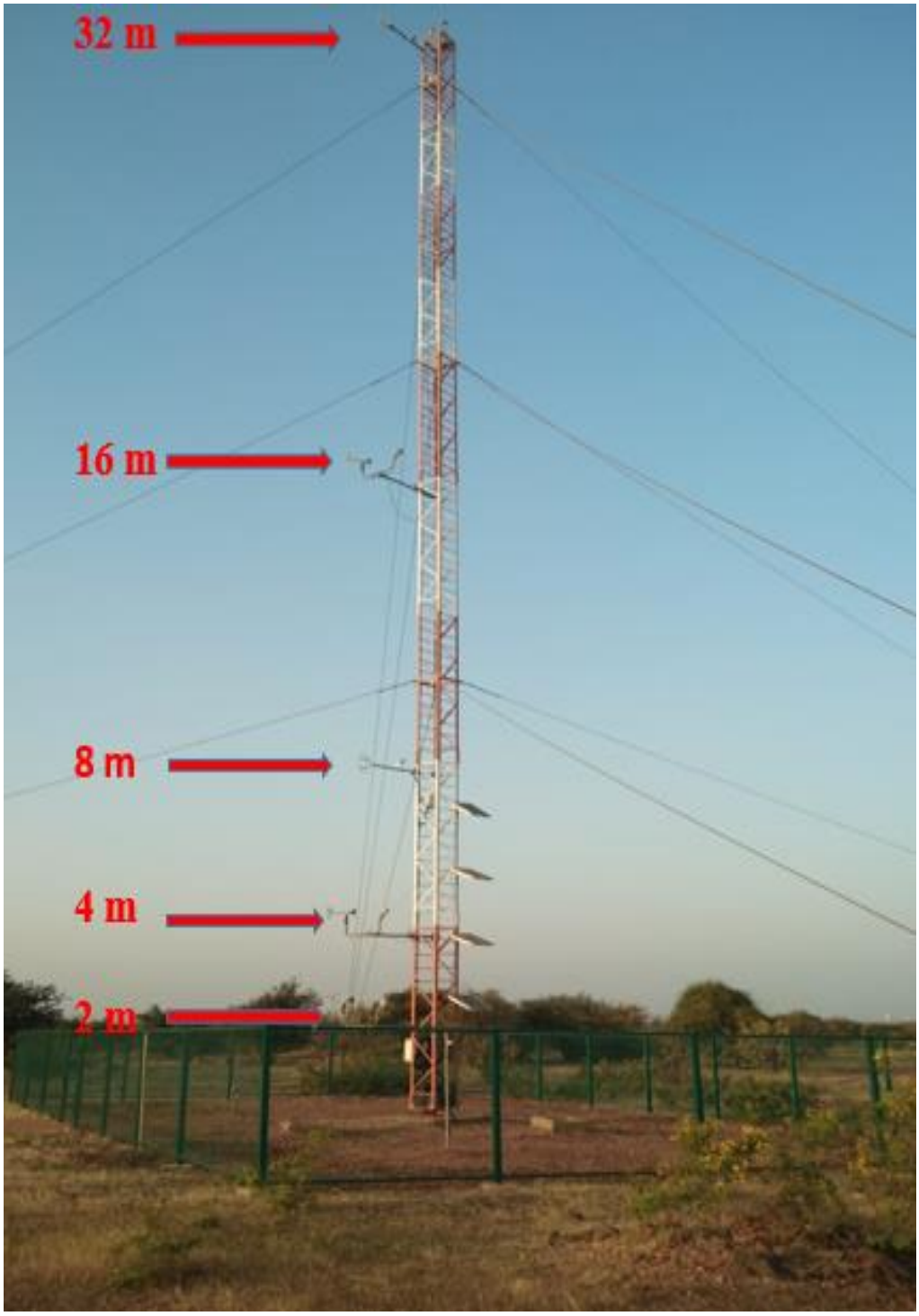

Fig. 9. Photograph of the 32-m ABL tower with the sensors mounted at 2 m, 4 m, 8 m, 16 m, and 32 m altitudes (marked by red arrows in the figure).

Table 2. Sensors deployed at different altitudes of the ABL tower

Parameter	Sensor	Altitude (m)	Make and model
Radiation	CNR4	2	Kipp and Zonen
Air temperature, relative humidity	CS215-L120-PT	2, 4, 16	Campbell Scientific, CS215
Wind speed and Direction	05103-L120-PT CSAT3A	2, 4, 16 8, 32	R. M. Young, 05103 Campbell Scientific
Pressure	CS100	2	Campbell Scientific

3.3.2.1 Radiation

Short wave and long wave radiation measurements are carried out by a pair of pyranometer and pyrgeometer kept in a similar configuration, one facing upwards and the other facing downwards (shown in Fig. 10). The CNR4 body contains two temperature sensors, a platinum resistance thermometer (Pt-100) and a thermistor which have a high degree of accuracy over a wide range of temperature, are integrated for compatibility with every data logger (Kipp and Zonen, 2009). In order to correct the infrared readings for the temperature of the instrument housing, the temperature sensors are build inside. For improving the quality of the temperature measurements, the temperature sensors should be kept in close association with the long wave sensors. The spectral range of the pyranometer ranges from 0.3 to 3 microns and that of pyrgeometer from 4.5 to 42 microns. The operating temperature of CNR4 lies between -40 to 80 °C. CNR4 has a field of view of 180° provided by the meniscus dome present in the upper long wave detector of CNR4. Uncertainty in daily total of <5 % (95 % confidence level in pyranometer) and <10 % (95 % confidence level) in pyrgeometer respectively.

Fig. 10. Photograph of CNR4 net radiometer

Both the incoming and reflected short wave and long wave radiation is measured by a pair of pyranometer and pyrgeometer. The most significant application of CNR 4 net radiometer is to measure the net radiation at the earth's surface. The output is expressed in W m^{-2}. The design is very light weight and has an integrated sun shield which reduces the thermal effects on long wave and short wave sensors (Kipp and Zonen, 2009).

3.3.2.2 Air temperature and relative humidity

AT and RH are measured with a CS215 probe, which utilises a Sensirion SHT75 sensor element. In order to measure RH, a capacitive sensor is built like a parallel plate capacitor. The sensing element serves as the dielectric. As the

moisture present in the air changes with the water vapour, the sensor adsorbs water into the humidity sensing material and thus results in the change in the dielectric constant. Dielectric constant is directly proportional to the capacitance which in turn is inversely proportional to the RH. For avoiding the direct effects of sunlight, the CS215 is housed inside a radiation shield. AT is measured within a range of -40 to +70 °C with an accuracy of ±0.3 °C (at 25 °C), ±0.4 °C (over 5 to 40 °C) and ±0.9 °C (over –40 to 70 °C). Measurement range of RH is 0 to 100 % with and accuracy of ±2 % (over 10 to 90 %) and ±4 % (over 0 to 100 %) at 25 °C.

3.3.2.3 Wind speed and direction

A helicoid shaped, four-blade propeller (shown in Fig. 11) is used for the measurement of horizontal WS and WD. A sensor in the form of a propeller measures the WS and a vertical tail provides the WD. Propeller blades rotate at a rate corresponding to the WS. A wind vane is positioned in the opposite side of the blade and forces the body to turn and face in the WD. A signal proportional to the WS is produced as a result of the propeller rotation. An R.M. Young 05103 sensor with an operating temperature range -50 – +50 °C, overall height 37 cm, 1.5 Kg weight and propeller diameter of 18 cm was used to study the mean wind speed and direction. WS ranging from 0 to 100 m s^{-1} can be measured with an accuracy of ±3 m s^{-1} and a starting threshold of 1 m s^{-1}. In the case of WD, the accuracy is ±3 m s^{-1} but with a starting threshold of 1.1 m s^{-1} ranging from 0° to 360°.

Fig. 11. Photograph of R.M.Young wind monitor mounted on a cross arm.

3.3.2.4 IRGASON (Integrated Open Path Gas Analyser and Sonic Anemometer)

IRGASON refers to Integrated Open Path CO_2 /H_2O Gas Analyser and 3D Sonic Anemometer. Both the gas analyser and the sonic anemometer are integrated in one sensor. The basic parameters that can be measured by IRGASON includes the CO_2 and water vapour densities, AT, barometric pressure, sonic air temperature, and three-dimensional WS. Three dimensional WS can be measured by three pairs of transducers placed in three different axes. Operating temperature ranges from -

30 to +50 °C. It operates by measuring the time taken by a high frequency (20 Hz) sound pulse to travel between a pair of transducers. Depending on the wind velocity, there will be variations in the time taken by the acoustic pulses to reach the other side. The relationship between AT, speed of sound (C_s), and the specific humidity (q) within the atmosphere is expressed as (Burns *et al.*, 2012),

$$AT = (C_s^2/(\gamma_d R_d)) (1/(1+0.51q)) \quad (10)$$

where γ_d is the dry air specific heat ratio and R_d is the gas constant for dry air.

Sound pulses are sequentially transmitted and received by transducers separated by a path length. The velocity component V_d along the path length (d) can be expressed as (Kaimal and Finnigan, 1994),

$$V_d = (C_s^2/2d) (t_2 - t_1) \quad (11)$$

where t_1 and t_2 are the transit times for sound pulses travelling downwind and upwind along parallel paths. V_d reduces to the measurement of (t_2-t_1), a relatively simple method of time interval measurement, if C_s and d are known.

3.3.2.5 Atmospheric pressure

CS100, which consists of a capacitive pressure transducer, is used for the barometric pressure measurements that ranges from 600 to 1100 mb. The capacitive transducer is housed with two parallel, closely spaced, and electrically separated metallic surfaces. One of the metallic surfaces is a diaphragm. Changes in the atmospheric pressure will be detected by the diaphragm and are converted into voltage signals. The resolution of the instrument is 0.01 mb and the accuracy ranges from ±0.5 mb at 20 °C, ±1.0 mb at 0 °C – +40 °C, ±1.5 mb at -20 °C – +50 °C, ±2.0 mb at -40 °C – +60 °C.

3.4 Data quality check

Sudden shoots in the measured data, known as spikes, can arise either from instantaneous large variations in the measured parameter or due to instrumental

error. The spikes and other noises present in the data have been screened mainly by:

- ❖ Manual screening
- ❖ 2-Sigma screening

Manual screening refers to the primary screening process done for removing the outliers or the spikes present in the raw data. Data points which are above or below the threshold (lower and upper) values were screened out. Common quality check protocols were imposed on the data. The threshold values for AT, horizontal wind speed, vertical wind speed and BC were set to 0–50 °C, ± 50 m s^{-1}, ±10 m s^{-1} and 0–10 µg m^{-3} respectively.

Following this, the next screening procedure followed was to remove the data points present outside two standard deviations from the mean values (2-sigma screening). Using a 30-minute averaging window, data points outside two standard deviations (σ) from the mean values (µ) were removed. The rationale behind selecting the 30-minute averaging period was to ensure that the atmospheric flows remain stationary (Bhat and Arunchandra, 2008), which is a necessary requirement in turbulence studies. Data points within the range of ($\mu \pm 2\sigma$) only were considered for further analysis. Data points outside ($\mu \pm 2\sigma$) were identified as outliers and were screened out. Spikes in the BC data were also removed using a 30 minute averaging window along with setting the threshold range ($\mu \pm 2\sigma$). Only the data points satisfying all the above-mentioned quality check criteria were used in the present study.

CHAPTER 4

RESULTS AND DISCUSSION

4.1 Atmospheric boundary layer dynamics and air quality

Data of continuous and collocated near-real time measurements of BC and ABL have been used to study the role of ABL dynamics in modulating the air quality (represented using BC) at this semi-arid, inland location, Challakere, in peninsular India. The diurnal and seasonal variations of BC and background meteorological parameters like AT, RH, WS, WD, and SW_{down} are also discussed.

4.1.1 ABL characterisation

For studying the role of ABL dynamics in modulating the air quality, it is necessary to know the characteristics of ABL at the study location. As mentioned in Chapter 3, the data collected using a dedicated 32-m tower having sensors at five altitudes form the basis for the ABL measurements. Meteorological parameters were measured continuously throughout the study period using slow response sensors (1/60 Hz). The data were subjected to quality check measures detailed in Chapter 3. The screened data were averaged over 30-minute intervals and used for further discussions.

4.1.1.1 Diurnal variation in downwelling shortwave solar radiation

The diurnal variations in SW_{down} for a representative clear sky and a cloudy day are shown in Fig. 12. Clear sky day is marked with a typical inverted-U pattern whereas the cloudy days are marked by occasional dips and higher fluctuations. The dips in SW_{down} may be attributed to the presence of clouds, which blocks the surface-reaching solar radiation partially. All the MLH estimates for the present study were made during clear sky days as the ABL characteristics are mainly governed by the incoming solar radiation and clear sky conditions ensure fully evolved boundary layers. Therefore JJAS season is not included in the present study to study dispersion. It should be noted that even though only clear sky days have

been used in the MLH estimates, the background meteorology analyses have been carried out for all sky conditions.

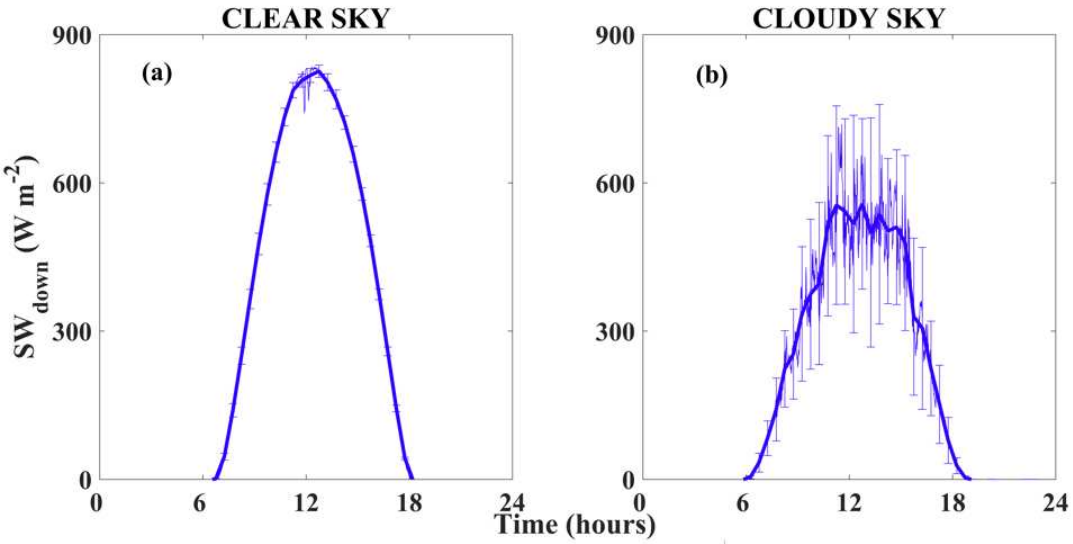

Fig. 12. Diurnal variations in SW_{down} for representative (a) clear sky and (b) cloudy sky days. The solid lines represent the 30-minute mean values and the vertical lines represent the standard deviation.

Seasonal diurnal variation in (SW_{down}) is shown in Fig. 13. Highest peak monthly mean solar irradiance (≈ 900 W m^{-2}) is attained in MAM and minimum in JJAS (≈700 W m^{-2}). Fluctuations are highest during JJAS and lowest during the MAM, highlighting the role of clouds in perturbing the SW_{down} pattern in JJAS and its influence in the evolution of daytime ABL. As expected, SW_{down} seems to be very low during JJAS season as the sky is overcast and starts to increase from ON, reaching a maximum value of around 900 W m^{-2} during MAM seasons.

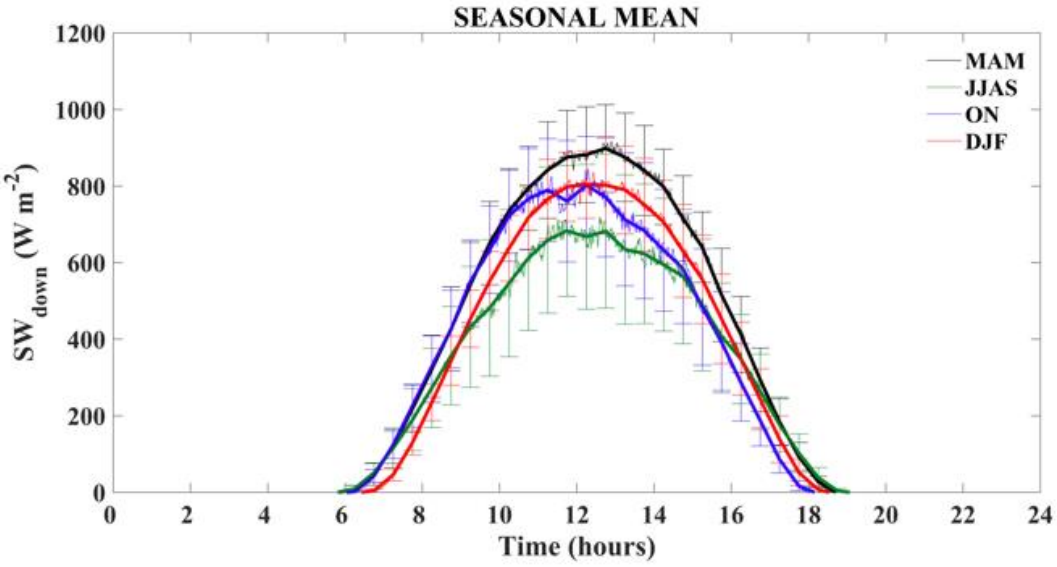

Fig. 13. Seasonality in the diurnal variations of surface reaching shortwave solar radiation. Smooth solid lines represent the 30-minute averages of 1-minute observations. The vertical lines denote the standard deviation values.

4.1.1.2 Air temperature and relative humidity

The half hourly averaged values of AT at 2 m, 4 m and 16 m above the ground for each month and season are shown in Fig. 14 and 15 respectively. From Fig. 14, maximum AT is observed during the month of April and minimum during January. The AT values at different heights above the ground show a diurnal pattern, as expected. It gradually rises from a minimum value before the sunrise to attain a peak between 14:00 to 16:00 hrs local time (LT) during all the months. From the late afternoon till the next sunrise, AT steadily decreases. The minima in AT is not much prominent from June to September. This is due to the cloudy skies, increased precipitation and strong winds during these seasons. Change in soil moisture characteristics leads to increased evaporation and interferes with the rapid heating and cooling of the air. Overcast sky results in lower surface temperature during day but higher at night which results in lower amplitude in diurnal pattern of AT during JJAS. AT reaches as high as 40 °C during April and below 20 °C during January. During all the months, maximum temperature is observed at 2 m height during the morning hours and at 16 m during the night. This is due to the

difference in the incoming solar radiation and land-atmosphere temperature. After sunset, temperature inversion occurs close to the surface, and the difference between incoming and outgoing radiation becomes negative due to the cessation of solar radiation and the emission of long wave radiation. So, the surface cools to a temperature below that of the air above it. Soon after sun rise the surface temperature increases and net radiation becomes positive. The peak value decreases as the height increases during daytime and is clearly visible in Fig. 14 and 15.

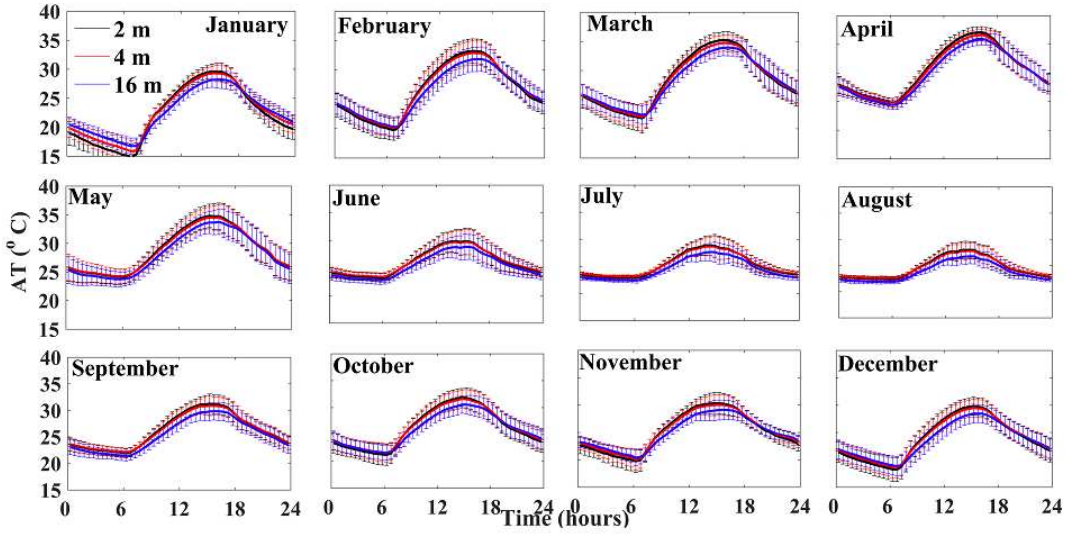

Fig. 14. Diurnal variations in AT for all months. The smooth solid lines represent the 30-minute averages of the 1-minute observations and the vertical lines represent the standard deviation values.

AT attains its maximum peak value during MAM due to high surface temperature as dry soil conditions prevails in the study region and the enhanced convective activities, and lowest during JJAS and DJF. The peaks are not much prominent during monsoon season.

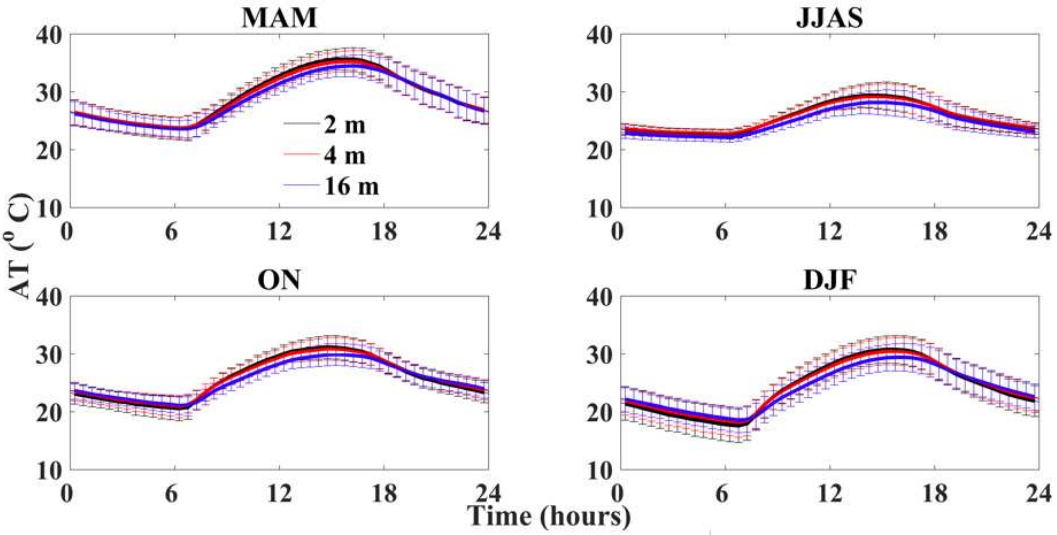

Fig. 15. Seasonality in the diurnal variation of AT. The smooth solid lines represent the 30-minutes averages of the 1-minute observations. The vertical lines represent the corresponding standard deviation values.

The seasonal mean diurnal variation of RH is shown in Fig. 16. RH varies in the range of 20% to 90% during different seasons. Maximum value of RH was 90% during JJAS and lowest value below 30% DJF and MAM (Fig. 16). As the region is dry and also less water vapour content results in very low RH during MAM, DJF and ON. By comparing the Fig. 4 and 5 the inverse relationship between the AT and RH can be clearly analysed. RH was observed to be very high during JJAS as expected.

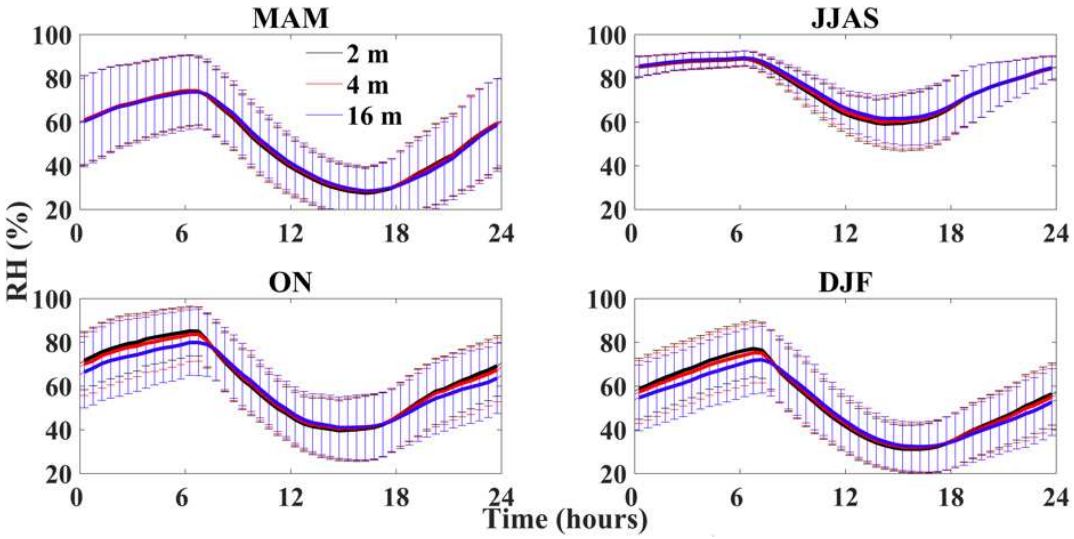

Fig. 16. Seasonality in the diurnal variation of RH. The solid lines represent the 30-minutes average and the vertical lines represent the standard deviation values.

4.1.1.3 Monthly and seasonal variations in the diurnal pattern of wind speed and direction

WS and WD plays a significant role in reporting air quality. WS and WD at a particular location over a time period can be graphically displayed in the form of a wind rose. Polar coordinate system is used in the wind rose diagram whereby the data is plotted at an angle relative to north and away from the origin. Each concentric circles in wind rose shows the frequency of time the wind blows from each direction and the length of spokes from a direction shows the percent of time wind comes from that direction. Colour bands present in the spoke provides how often wind blows in each pre-defined WS range (bins) represented in m s^{-1}.

The diurnal variation in seasonal mean WS and WD is shown in Fig. 17 to 20. WS, in general, are benign during DJF and ON seasons and follow an increasing pattern from MAM, marking the onset and strengthening of the strong Indian Summer Monsoon (ISM) winds, following which the wind speeds start decreasing again. WS is highest at 16 m, intermediate at 4 m and lowest at 2 m (out of the measurements reported in this study), with a clear positive gradient in WS along the vertical direction. In general, the WS within the surface layer is expected to

increase with respect to the increase in altitude. The frictional drag imposed by the underlying rigid surfaces has an abundant control over the wind flow in the boundary layer. The movement of the winds close to the ground is retarded by the frictional drag and the horizontal wind speed gets reduced as it approaches the surface. And due to the reduced frictional drag at higher altitudes, the WS increases as the altitude increases. This is observed during all months and seasons which is depicted in Fig. 17 to 20. The turbulent mixing present in the day-time convective boundary layer makes the wind profile nearly steady with respect to the increase in the height. The wind speed varies with respect to the characteristics of the terrain and the stability conditions of the atmosphere (Oke, 1978).

During DJF (shown in Fig. 17), winds blow from eastern and south eastern side with WS showing a clear diurnal pattern at all the three altitudes mentioned. Weak winds with a WS of the range 0.6 to 1 m s^{-1} were observed at 2 m height with a frequency of 23.75 % of time along with a WS of the range 2 to 2.2 m s^{-1} from south eastern side. At 4 m and 16 m height the WS in the range of 2.2 to 2.4 m s^{-1} and 3 to 3.2 m s^{-1} were predominant at 34.5 and 29 % of time respectively. Following DJF season, the MAM (shown in Fig. 18) starts, diurnal variations in WS and WD starts diminishing and slowly approaches towards the direction characteristic to ISM. Influence of both south easterlies and south westerlies were observed during MAM. The winds blow from south western side at speeds between 1.7 to 1.9 m s^{-1} about 5.25% of the time, 2.5 to 2.7 m s^{-1} about 8.25 % of the time and in the range of 2 to 2.4 m s^{-1} about 21.25 % of the time at 2 m altitude. A maximum WS of 3 m s^{-1} about 9 % of the time at 4 m and 4.2 to 4.4 m s^{-1} about 3 % of the time at 16 m altitude were observed. Lowest WS at 16 m altitude were in the range of 2.8 to 3.6 m s^{-1} about 26.25 % and 23.75 % of the time from south western and south eastern side respectively. Strongest winds which are directionally consistent without any diurnal pattern was observed during JJAS season (shown in Fig. 19). Maximum WS of 4.5, 5.5 and 7 m s^{-1} were observed at 2, 4, and 16 m about 37 %, 20 % and 30 % of time respectively. As ON (shown in Fig. 20) begins, the WS and WD reverts back to have diurnal variations with a decreased WS as compared to JJAS. South easterlies with a WS between 0.6 to 1.3 m s^{-1} about 21.25

% of time at 2 m height, 0.5 to 1.5 m s^{-1} about 21 % of time at 4 m and between 1.5 to 2.5 m s^{-1} about 24 % of time was observed at 16 m respectively. Influence of easterlies with an increased WS between 1 to 2.4 m s^{-1}, 1.2 to 2.7 m s^{-1} and 2.5 to 3.8 m s^{-1} were observed at 2, 4 and 16 m altitudes respectively.

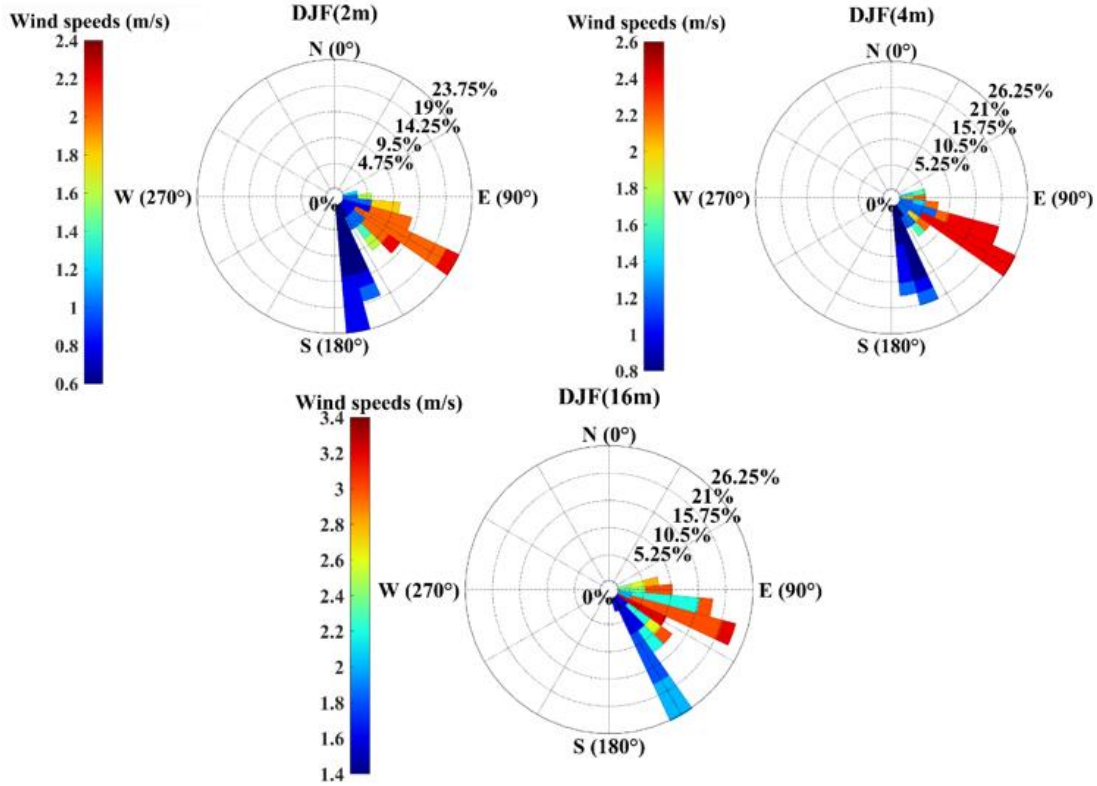

Fig. 17. Diurnal variation of WS during DJF. Each concentric circle shows the frequency of wind. Spokes around the circle shows how often wind blew from each direction along with the pre-defined WS. Colour bar present at the side of wind rose gives the WS in m s^{-1} categories along with their associated colours.

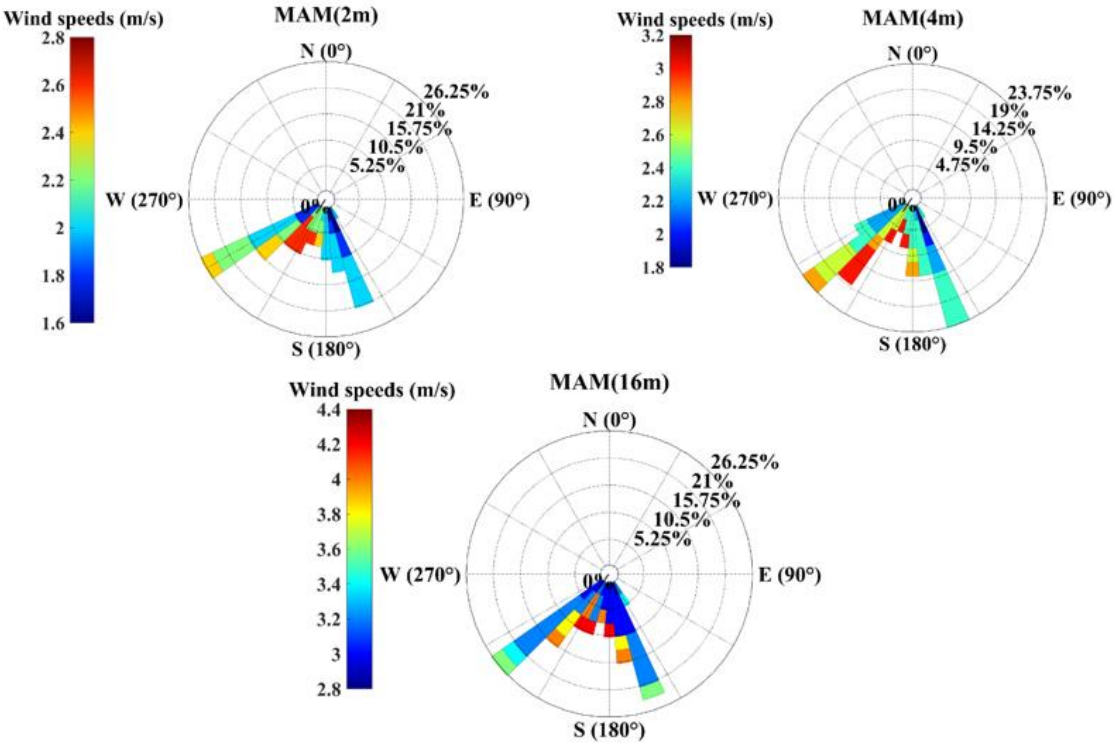

Fig**.** 18. Diurnal variation of WS during MAM. Each concentric circle shows the frequency of wind. Spokes around the circle shows how often wind blew from each direction along with the pre-defined WS. Colour bar present at the side of wind rose gives the WS in m s^{-1} categories along with their associated colours.

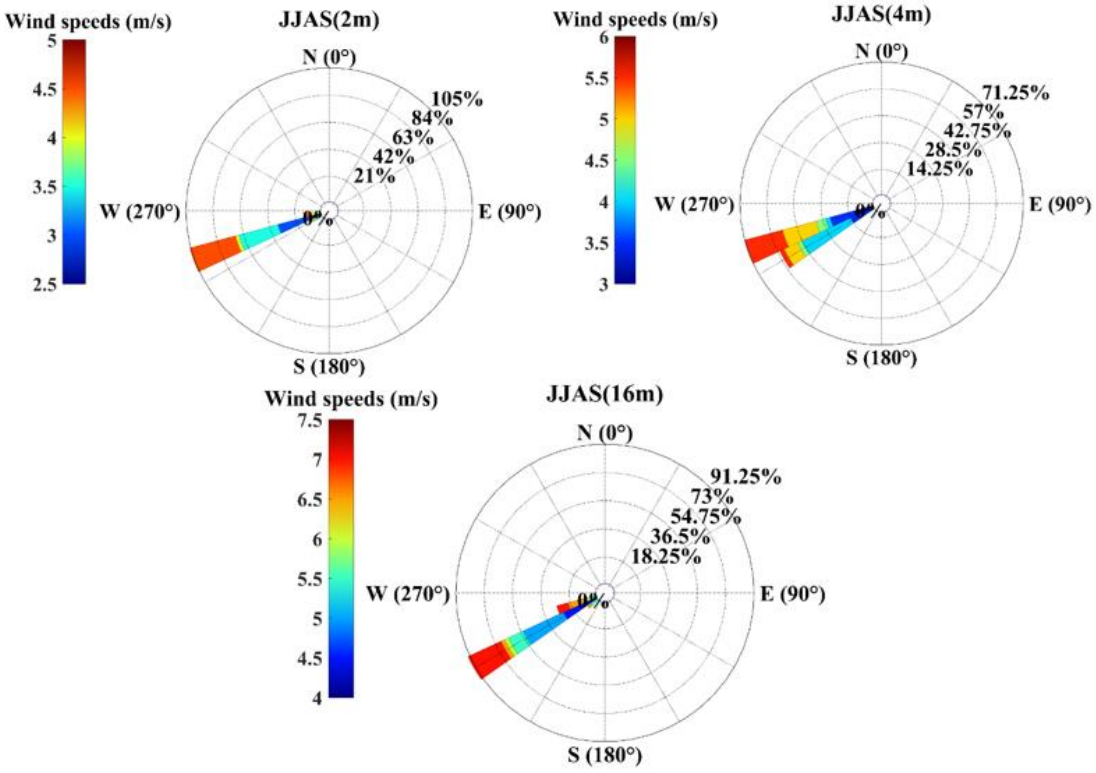

Fig**.** 19. Diurnal variation of WS during JJAS. Each concentric circle shows the frequency of wind. Spokes around the circle shows how often wind blew from each direction along with the pre-defined WS. Colour bar present at the side of wind rose gives the WS in m s^{-1} categories along with their associated colours.

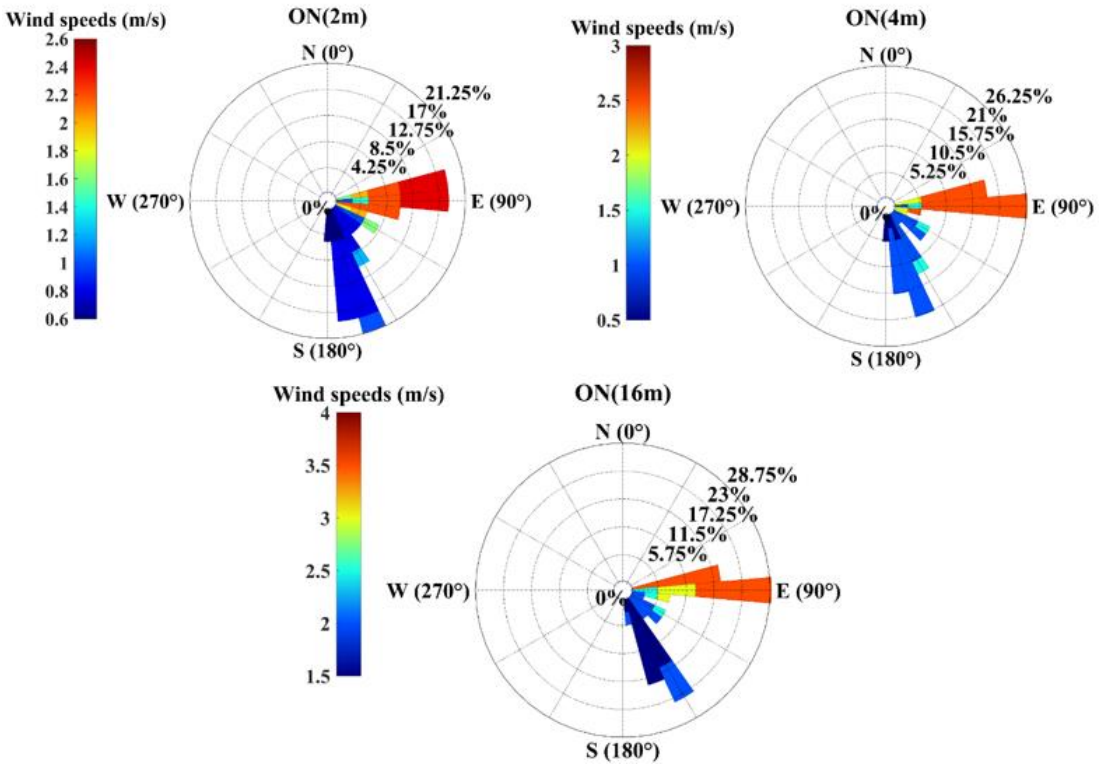

Fig**.** 20. Diurnal variation of WS during ON. Each concentric circle shows the frequency of wind. Spokes around the circle shows how often wind blew from each direction along with the pre-defined WS. Colour bar present at the side of wind rose gives the WS in m s^{-1} categories along with their associated colours.

4.1.2 Temporal variation of mixing layer height (MLH)

As mixing layer serves as the atmospheric volume available for the redistribution and dilution of the pollutants close to the surface, information regarding the diurnal variations of MLH is crucial for air quality characterisation. Temporal variations in MLH during daytime for 10 clear sky days of DJF, MAM and ON seasons are shown in Fig. 21. As expected, during all the seasons, MLH starts gradually increasing after the sunrise, reaching maximum values in the afternoon, and starts to decrease on approaching towards the sunset. Maximum peak in MLH was observed during MAM, followed by ON and the least during DJF due to the variations in the strength of convection prevailing in the region with respect to the seasons. MLH follows well-defined diurnal pattern with an increase from

MLH values at 09:00 hrs LT to peak within 14:00 to 16:00 hrs LT with an average value of ~1900 m (during MAM season). Following the peak, it decreases rather faster (as compared to the growth) to attain a minimum value of ~300 m close to 19:00 hrs; possibly marking the growth phase of a stable, NBL. During ON and DJF seasons, the maxima in MLH corresponds to ~1600 m and ~1400 m respectively. The maximum peak of MLH during all the three seasons reported seems to be shifted a few hours in the late afternoon as compared to that of the maximum peak of solar radiation. This can be explained by the specific heat capacity of the ground in response to the incoming solar radiation. The observed high MLH peak during MAM is attributed to the strong convective activities (high incoming solar radiation during MAM) which leads to enhanced turbulence. Being a semi-arid region, high convective lifting time during MAM season can be observed. MLH during ON and DJF is affected by low surface temperature patterns, reduction in the ground-reaching solar radiative flux which results in reduced convective activity, and the reduced WS leads to suppressed mechanical turbulence. Thus it can be said that the diurnal variation in MLH mainly depends in the local topography, synoptic conditions as well as the topography of the area. The influence of SW_{down}, surface temperature and WS in the development of MLH is reported in studies presented by Holzworth, (1967); Murthy *et al.*, 1980; Mues *et al.*, 2017.

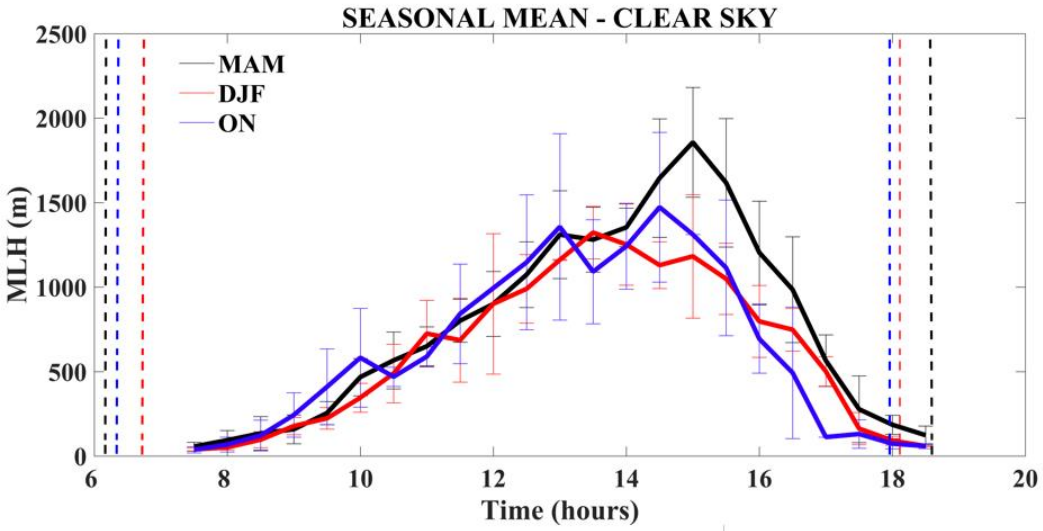

Fig. 21. Diurnal variation of seasonal mean of MLH. The dashed vertical lines represent the seasonal mean sunrise and sunset times. The vertical lines represent the standard deviation.

Kompalli *et al*. (2013) reported a very high seasonal mean MLH value of 3014 ± 1187 m during MAM, followed by 1871 ± 506 and 1488 ± 706 m during ON and DJF respectively over Nagpur in Central India which is high as compared to that of the present study. Observations made by Krishnan and Kunhikrishnan, (2004) over Gadanki, a tropical Inland station situated in South Eastern part of India reported high values during MAM (2200 ± 420 m), followed by ON (1680 ± 350 m) and DJF (1500 ± 340 m). However, the present study differed from the results reported over Kadapa (Begam *et al*., 2016), a tropical semi-arid location in Southern India with an average peak height maxima during MAM (3000 ± 200 m), followed by DJF (1800 ± 300 m) and ON (1700 ± 300 m). All these MLH characterisations portray the spatial and seasonal variations of MLH.

4.1.3 Monthly diurnal variation of BC

Near-surface concentration of BC was measured every minute; the diurnal variations in the monthly averaged BC is shown in Fig. 22. Half hour averaged values of the BC concentration along with their standard deviation values are shown

in Fig. 22. The major observations from the diurnal variation of BC concentration for all months are:

- A sharp shoot in BC concentration during the morning hours, during 08:00 hrs LT (known as the fumigation peak). The fumigation effect brings the pollutants present in the RL to near surface (Stull, 1988) which will be explained in detail in the next section.
- Following the peak, BC mass concentration gradually decreases to minimum during the afternoon hours around 16:00 hrs LT attributed to higher surface temperature as the day advances, increased convective activity, and high WS.
- During the late evening hours, BC concentration starts increasing and remains at higher values throughout the night due to the prevailing stable atmospheric conditions and also low WS.
- Conspicuous diurnal pattern has been observed from November to March. This can be explained with the help of prevailing synoptic meteorological conditions of the area which includes scanty rainfall, very weak winds, diurnal oscillations in the temperature, altogether contributing to stable atmospheric conditions.
- May to September months are devoid of large diurnal variations. Among all the months, least BC mass concentration was observed during August when the region experiences low temperature, high rainfall and strong winds which leads to the wash out of aerosol particles.

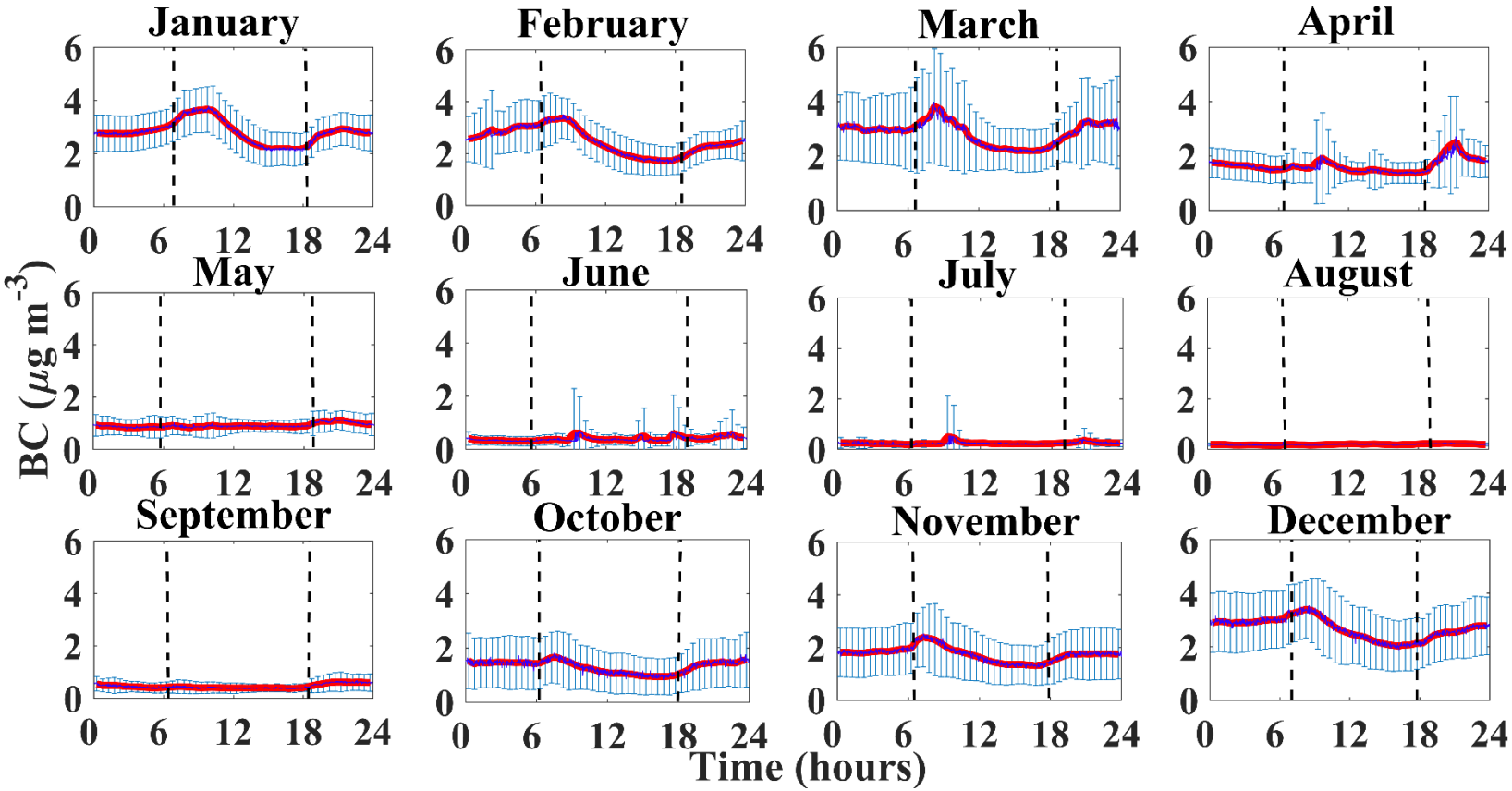

Fig. 22. Diurnal variation of BC for all the months. The solid red lines represent the 30-minutes average of the observations and the blue vertical lines represent the standard deviation values. The vertical dashed lines represents the monthly mean sunrise and sunset times.

Table 3. Monthly mean values of BC measured during the study period.

Month	**BC mass concentration (µg m^{-3})**
January	2.80 ± 0.43
February	2.48 ± 0.52
March	2.79 ± 0.38
April	1.61 ± 0.20
May	0.91 ± 0.02
June	0.37 ± 0.05
July	0.23 ± 0.02
August	0.19 ± 0.02
September	0.44 ± 0.08
October	1.30 ± 0.28
November	1.74 ± 0.27
December	2.67 ± 0.39

The annual average BC mass concentration in Challakere during the study period was observed to be 1.47 ± 0.18 µg m^{-3} which is similar to those reported at semi-arid, dry, continental location Anantapur (Kumar *et al.*, 2011) and Nainital, located in Shivalik range of central Himalayas (Pant *et al.*, 2006) with an annual average BC mass concentration of 1.97 ± 0.12 µg m^{-3} and 1.36 ± 0.99 µg m^{-3}. However, this value is much lower when compared to other locations like Delhi (Tiwari *et al.*, 2013), Nagpur (Kompalli *et al.*, 2014), tropical semi-arid location in southern India, Kadapa (Begam *et al.*, 2016), and a tropical urban location Hyderabad (Dumka *et al.*, 2013) with an annual average BC mass concentration of 6.70 ± 5.70 µg m^{-3}, 3.09 ± 1.28 µg m^{-3}, 2.20 ± 0.78 µg m^{-3}, and 4.45 ± 0.12 µg m^{-3} respectively. It is higher when compared to a rural high-altitude station like Nainital (0.99 ± 0.02 µg m^{-3}) reported by Dumka *et al*. (2010). Table. 3 shows the monthly mean values of BC along with their standard deviation values, calculated from the BC measurements carried out during the study period. From Table. 3, it can be seen that the BC concentration varied from a monthly mean low value of 0.19 ± 21.84

μg m^{-3} during August to a high value of 2.80 ± 0.43 μg m^{-3} during January, showing large monthly variations.

4.1.4 Seasonality in the diurnal variation of BC

Fig. 23. shows seasonality in the diurnal variation of BC. The major observations from the seasonal variation of BC concentration are as follows.

- A sharp shoot in BC concentration is observed during the morning hours within one hour after sunrise, around 08:00 hrs LT, mainly during DJF and ON. The interaction of solar radiation with the ground after the sunrise heats the ground, which results in the rising of thermals, thereby deepening the ABL by breaking the inversion layer. Hence, the mixing of the pollutants in the nighttime residual layer happens with the growing mixing layer, thereby increasing the near-surface aerosol concentration, and forms the fumigation peak (Stull, 1988).
- A gradual decrease to minimum concentration during the afternoon hours, (around 16:00 hrs LT) and then a gradual increase to attain a constant high value which remains throughout the night. Due to the strong convective mixing during the day time, ABL deepens until evening, which increases the volume available for effective dispersion of near-surface BC particles, thereby diluting its near-surface concentration. As the day advances, the radiative cooling of the surface during the late evening hours, which continues until nighttime, leads to the formation of a shallow stable boundary layer which causes the confinement of BC particles within the near surface. Limited anthropogenic activity (Anand *et al.*, 2020) along with a large fraction of submicron particles (Satheesh *et al.*, 2013), the gravitational settling of particles will not be not much pronounced in the study region. Therefore a constant high concentration was observed throughout the night.
- The second prominent peak can be observed in the evening hours during MAM, between 20:00 – 23:00 hrs LT, which decreases gradually thereafter till the next sunrise. The increased WS during MAM season results in the long-range

transport of pollutants. As strong winds carry away most of the BC particles, lower near-surface BC concentration was observed during MAM.

- The diurnal pattern is most conspicuous during ON and DJF. The seasonal mean BC mass concentration was observed to be higher in DJF followed by MAM and ON, and the lowest values were observed during JJAS (Fig. 23). During DJF, reduced convective mixing, and shallower ABL results in the increased concentration of near-surface aerosols. Weak winds increases the residence time of the BC particles. During MAM, enhanced convective mixing results in well-developed ABL due to which the pollutants gets lifted to larger heights.
- During JJAS, the BC concentration is extremely lower than that of MAM and DJF. Strong south westerly flows, bring forth rainfall with it as a part of the ISM. The wash out process, along with the strong winds, plays a significant role in the scavenging of the aerosol particles during JJAS season. In addition to low surface temperatures, high RH, change in the soil moisture conditions, and cloudy skies, inhibits the ABL dynamics.

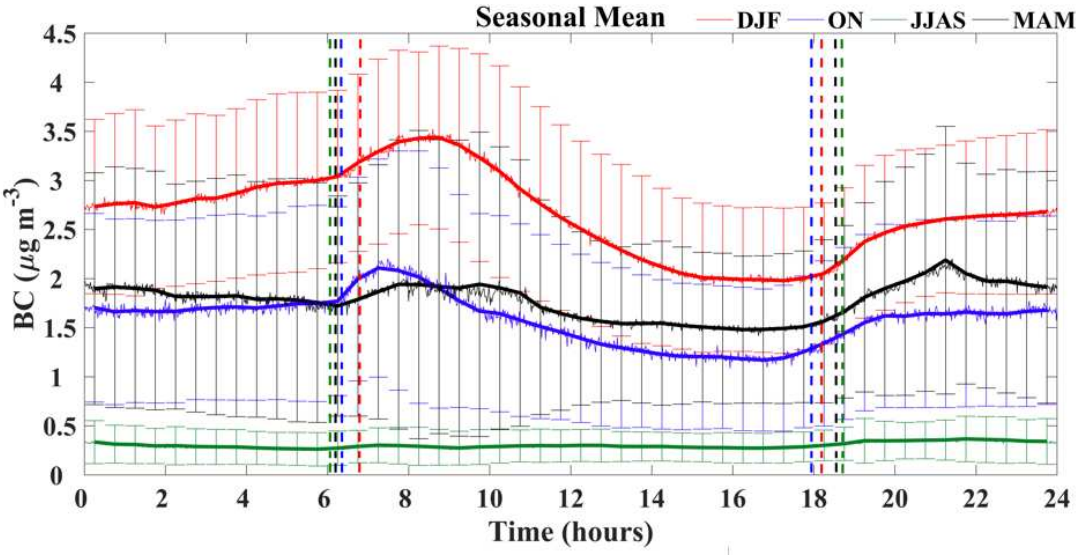

Fig. 23. Seasonality in the diurnal variation of BC. The smooth solid lines represent the 30-minute average of the 1-minute observations (light shaded lines). The dashed vertical lines represent the seasonal mean sunrise and sunset times. The solid vertical lines represent the standard deviation values.

Table. 4. Seasonal mean values of BC

Season	**BC mass concentration (µg m^{-3})**
DJF	2.65 ± 0.42
MAM	1.77 ± 0.18
JJAS	0.30 ± 0.02
ON	1.58 ± 0.24

From Table 4, the average BC concentration was observed to be the highest during DJF (2.65 ± 0.42 µg m^{-3}), followed by MAM (1.77 ± 0.18 µg m^{-3}), ON (1.58 ± 0.24 µg m^{-3}) and with the least values during JJAS (0.30 ±0.02 µg m^{-3}). These results are in agreement with those reported by Satheesh *et al*. (2013) and Anand *et al*. (2020) over the same study region, Challakere. As the study area is an inland location with less anthropogenic activities the seasonal variation in near-surface BC mass concentration will be due to the background meteorological conditions and long range transport processes. The diurnal variations in near-surface BC mass concentration is associated with the ABL dynamics (Babu and Moorthy, 2002; Babu and Moorthy, 2006; Nair *et al.*, 2007; Beegum *et al*., 2009; Dumka *et al.*, 2010; Kumar *et al.*, 2011; Dumka et al., 2013; Satheesh *et al.*, 2013; Begam *et al.*, 2016; Anand *et al.*, 2020). Even though the magnitude of BC differs in different regions, the seasonal variation with a high concentration in winter and lower in monsoon are observed at other locations of India, like the semi-arid rural location Anantapur (Kumar *et al*., 2011), semi-arid location Kadapa (Begam *et al*., 2016), and those from coastal stations like Thiruvananthapuram (Babu and Moorthy, 2002) and Chennai (Aruna *et al*., 2013). In contrast to this, Sarkar *et al*. (2014) observed a strong seasonal variation in BC with a maximum concentration during the MAM followed by DJF over a high-altitude station Darjeeling. This is explained by the increased anthropogenic activities, long range transport of the particles through air masses and the vertical advection of the pollutant particles (in the valleys) to higher altitudes.

4.1.4.1 Dependence of near-surface BC concentration to MLH

MLH is defined as the height of the layer adjacent to the SL, where vigorous mixing occurs due to convection and mechanical turbulence. It affects the vertical distribution of the atmospheric pollutants and water vapour. With a view to examining the relationship between BC concentration and MLH, scatter plots were made between them during all seasons and are shown in Fig. 24. Linear least square regression was carried out on the scatter plots, and the resulting Pearson's correlation coefficient (R) was calculated.

Correlation refers to a bivariate analysis which measures the strength and direction of relationship between two variables. The correlation coefficient varies from -1 to +1 which gives the degree of the association between the variables. A perfect degree of association between the variables are represented by a value of ± 1, where + sign represents positive relationship and - sign represents negative relationship. In statistics, different types of correlation are measured. In the present study, R, which is a widely used correlation statistic to measure the degree of relationship between linearly related variables, is used. R is calculated using the following formula (SPSS tutorials, n.d.),

$$R_{XY} = \frac{\sum_{i=1}^{n}(X_i - \overline{X})(Y_i - \overline{Y})}{\sqrt{\sum_{i=1}^{n}(X_i - \overline{X})^2}\sqrt{\sum_{i=1}^{n}(Y_i - \overline{Y})^2}} \quad (12)$$

where R_{XY} refers to the Pearson's correlation coefficient between X and Y, n is equal to the number of observations, and X_i and Y_i refers to the value of X and Y for i^{th} observation, and $\overline{X}$ and $\overline{Y}$ represents the mean of X and Y respectively. In this context, 'X' is represented by MLH and 'Y' by BC.

Regression analysis is mainly used to find the equations that fits the data. In simple linear regression, one independent variable X is plotted against one dependent variable Y. In Fig. 13. the relationship between BC and MLH is described by red downward slopping straight line. The equation for the line can be represented as,

$$Y = a + bX \quad (13)$$

Where 'Y' is the dependent variable, 'X' is the independent variable, 'b' is the slope of the line and 'a' is the y-intercept.

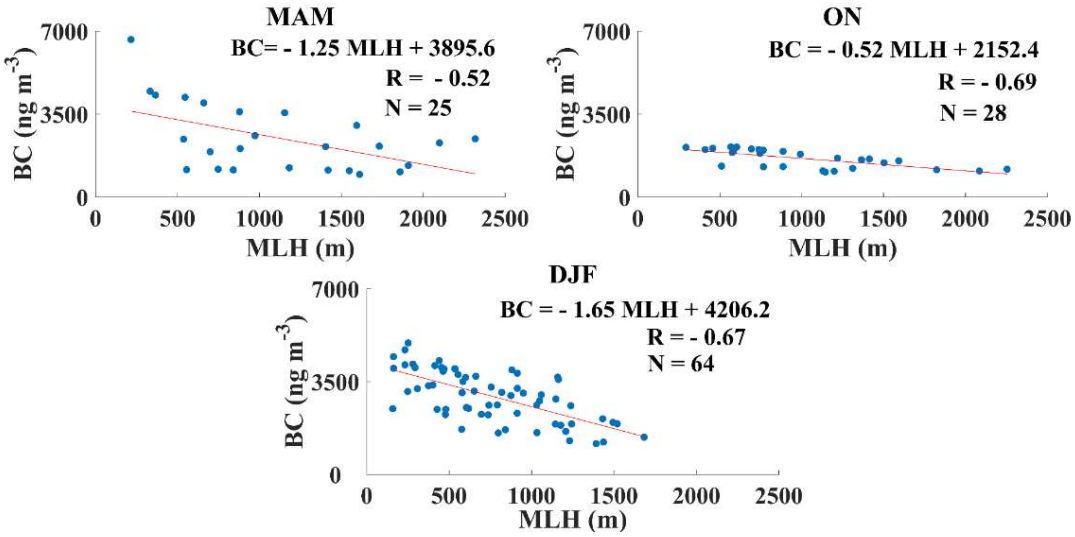

Fig. 24. Scatter plots between MLH and BC for ON, DJF, and MAM. The blue dots mark the individual scatter points and the solid red line represents the linear regression lines drawn through them. The linear fits and the number of data points (N) are shown in the corresponding panels.

From Fig. 24, it is seen that the BC concentration shows a linear relationship with MLH during MAM, ON and DJF and is given by eq. 14, 15 and 16 respectively. BC in 'μg m^{-3}' is the dependent variable or response variable and MLH in 'm' is the independent variable or predictor variable. The scatter plot with small blue dots represents the true value and red solid downward slopping line represents the linear model which minimises the sum of the squared length of the errors (error represents the distance between the point to the regression line). Or it can be said that it represents the line of best fit.

$$BC = -1.25 \times MLH + 3895.6 \quad (14)$$

$$BC = -0.52 \times MLH + 2152.4 \quad (15)$$

$$BC = -1.65 \times MLH + 4206.2 \quad (16)$$

Table. 5. Correlation coefficients obtained from the least square linear regression fitting between BC-MLH for all seasons.

Season	**R**
DJF	-0.67
MAM	-0.52
ON	-0.69

During all the three seasons the slope was observed to be < 0 which shows the negative relationship between BC and MLH, ie., increase in MLH decreases BC. Table 5 shows the R between MLH and BC during DJF, MAM and ON pointing to the inverse dependency between convective lifting and near-surface aerosol concentration. As discussed in the earlier section the convective lifting increases the volume available for the mixing and dilution of pollutants to higher altitudes, thereby decreasing the near-surface concentration. Higher BC reduces the surface reaching solar radiation thereby influencing the diurnal evolution of ABL.

4.1.5 Dispersion of BC

For the better understanding of the dispersion of air pollutants (BC in this context) the calculation of the ventilation coefficient (VC) is necessary. The diurnal variations in VC during MAM, ON and DJF are shown in Fig. 25. To study the diurnal variation of VC, the MLH values for each day and the corresponding WS within the mixed layer are used. In the present study, day-time MLH values (representing fully evolved ABL) during clear sky days of MAM, ON and DJF are only used. In the present study, the average wind speed at 16 m altitude was utilized to represent the mean wind speed within the ML.

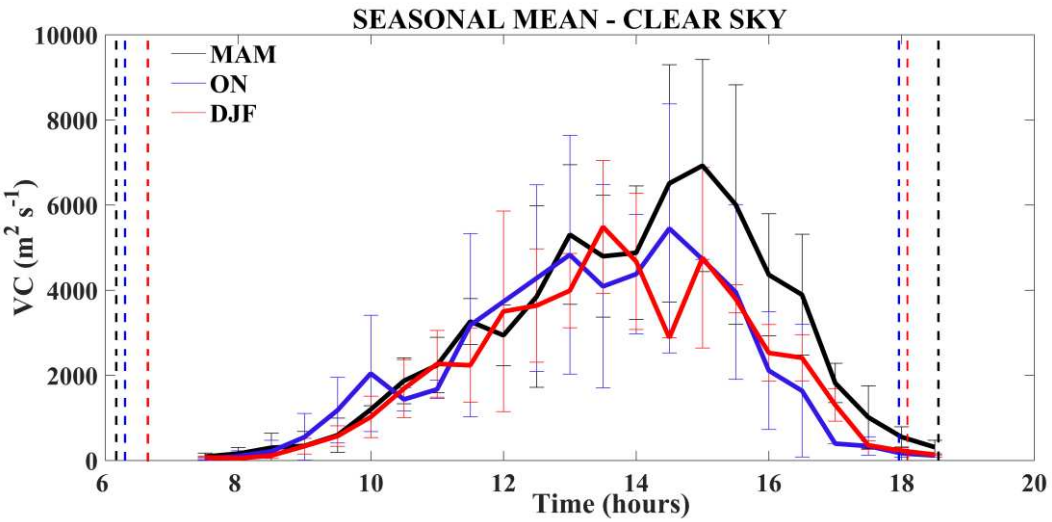

Fig. 25. Diurnal variation in VC for different seasons. The dashed vertical lines mark the seasonal mean sunrise and sunset times. The vertical lines represent the corresponding standard deviation.

Fig. 25 shows the diurnal variation of VC with a gradual increase after sunrise, from extremely low values, reaching maximum values around noon time, and then decreasing towards the sunset. The cessation of incoming solar radiation causes gradual decrease in VC. Following the sunset, the stable, ABL along with a reduced wind speed contributes to low VC during these hours. As VC represents the combined effects of advection and vertical mixing, higher value of VC during the noon time points to the higher dispersive capacity of the ABL. The diurnal pattern of VC was found to be same as that of MLH and WS. Maximum peak value was observed during MAM (~7000 m^2 s^{-1}), followed by ON (~5800 m^2 s^{-1}) and DJF (~5700 m^2 s^{-1}). The seasonal mean VC was observed to be highest during MAM (2751.3 ± 1006 m^2 s^{-1}), followed by ON (2133.8 ± 1036 m^2 s^{-1}) and DJF (2091.6 ± 665 m^2 s^{-1}). Higher VC values during MAM is due to the enhanced thermal convection (fully evolved MLH) and WS in the study area, which highlights the better dispersive capacity and low pollution potential during MAM, and the lowest VC during DJF is attributed to the shallower boundary layer height and weak winds prevailing in the region. Observations over Gadanki, a tropical inland station in southern India reported higher VC during MAM (10565 m^2 s^{-1}) and lowest during DJF (7405 m^2 s^{-1}) (Krishnan and Kunhikrishnan, 2004). Singh and Pandya, (2013)

reported a maximum value of VC during MAM (4719 m^2 s^{-1}), followed by ON (1852.5 m^2 s^{-1}) and DJF (1275 m^2 s^{-1}) respectively in a study over a coastal industrial city Mangalore.

4.1.5.1 Dependence of near-surface BC concentration to VC

In order to examine the relationship between VC and BC concentration, scatter plots were made between them during all seasons and are shown in Fig. 26. Linear least square regression was carried out on the scatter plots, and the resulting R values were calculated.

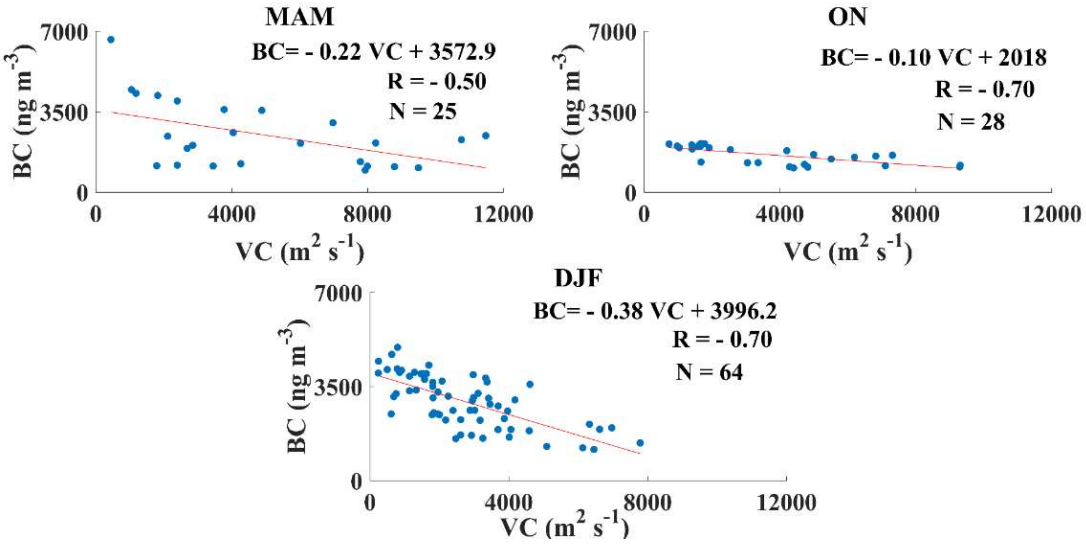

Fig. 26. Scatter plots between VC and BC for ON, DJF, and MAM. The blue dots mark the individual scatter points and the solid red line represents the regression lines drawn through them. The linear fits and the number of data points (N) are shown in the corresponding panels.

Eq. 17, 18, and 19 represent the linear fit equations between VC and BC during MAM, ON and DJF respectively,

$$BC = -0.22 \times VC + 3572.9 \quad (17)$$

$$BC = -0.10 \times VC + 2018.1 \quad (18)$$

$$BC = -0.38 \times VC + 3996.2 \quad (19)$$

Table. 6 Correlation coefficients obtained from the least square linear regression fitting between BC-VC for all seasons.

Seasons	**Pearson's correlation coefficient (R)**
DJF	-0.7
MAM	-0.5
ON	-0.7

Negative slopes during all the three seasons shows the inverse relationship between VC and BC. The negative slope and y-intercept is seen to be highest during DJF followed by MAM and ON. The number of data points used is represented by 'N'. By comparing Tables 5 and 6, the negative correlation is high in BC-VC relationship as compared to that of BC-MLH. This is due to the combined influence of MLH and WS (both having an inverse relationship with BC) in the case of VC.

In general, the dispersion of the pollutants is highly influenced by the prevailing meteorological parameters at the location. Out of these, the most significant are the wind speed and MLH, which represent the horizontal and vertical redistribution of the pollutants. Under unstable boundary layer conditions, VC will be high, therefore the air quality will be better with less pollution potential. However, under stable atmospheric conditions, VC will be least, with an increase in pollution potential and poor air quality. During MAM, the air quality will be better as compared to that of ON and DJF.

CHAPTER 5

SUMMARY AND CONCLUSION

Year-round continuous and collocated near-real time measurements of BC and ABL have been carried out to investigate the role of ABL dynamics in modulating the air quality (represented using BC) at a semi-arid, inland location in peninsular India. The main observations are as follows.

1. BC mass concentration was highest in DJF (2.65 ± 0.42 µg m^{-3}), lowest during JJAS (0.30 ±0.02 µg m^{-3}), and remained moderate during MAM (1.77 ± 0.18 µg m^{-3}), and ON (1.58 ± 0.24 µg m^{-3}) respectively.
2. BC was observed to show a well-defined diurnal variation with a morning peak (about one hour after the sunrise, around 08:00 hrs LT), followed by an afternoon low (between 14:00 to 16:00 hrs LT), and remains at higher values throughout the night during all the seasons. These are strongly associated with ABL dynamics.
3. During JJAS season, winds are strong and directionally consistent south westerly, while winds are weak and easterly/south easterly during DJF with diurnal variations.
4. The diurnal pattern was more pronounced with a high BC mass concentration during DJF due to the shallow ABL and low wind speed. While the diurnal pattern was subdued with lowest BC concentration during JJAS due to the strongest winds along with rainfall scavenging.
5. MLH showed a diurnal pattern with a maximum peak during MAM (~1900 m) followed by ON (~1600 m) and DJF (~1400 m). This is mainly due to the variation in the strength of convection during different seasons along with the synoptic meteorological conditions of the region.
6. VC values was found to be highest during MAM (2751.3 ± 1006 m^2 s^{-1}), followed by ON (2133.8 ± 1036 m^2 s^{-1}) and DJF (2091.6 ± 665 m^2 s^{-1}). Seasonal variation of VC suggests that the dispersion was highest during MAM and lowest during DJF.

7. A negative correlation between MLH-BC and VC-BC was observed during DJF, MAM, and ON. This highlights the inverse relationship of BC with MLH and WS.
8. Air quality will be better during MAM and poor during DJF and ON which is evident from the seasonal mean values of VC.

REFERENCES

Adopted, I.P.C.C., 2014. Climate Change 2014 Synthesis Report.

Afroz, R., Hassan, M.N., and Ibrahim, N.A. 2003. Review of air pollution and health impacts in Malaysia. *Environ. res.* 92(2): 71-77.

Ahrens, C. D. 2012. *Meteorology today: an introduction to weather, climate, and the environment* (9th Ed.). Cengage learning, United States of America, 549p.

Alappattu, D.P. and Kunhikrishnan, P.K. 2010. Observations of the thermodynamic structure of marine atmospheric boundary layer over Bay of Bengal, Northern Indian Ocean and Arabian Sea during premonsoon period. *J. Atmos. Sol.-Terr. Phys.* 72: 1318–1326.

Anand, N., Sunilkumar, K., Satheesh, S.K., and Moorthy, K.K. 2020. Entanglement of near-surface optical turbulence to atmospheric boundary layer dynamics and particulate concentration: implications for optical wireless communication systems. *Appl. Opt.* 59(5): 1471-1483.

Aruna, K., Kumar, T.L., Rao, D.N., Murthy, B.K., Babu, S.S., and Moorthy, K.K. 2013. Black carbon aerosols in a tropical semi-urban coastal environment: Effects of boundary layer dynamics and long range transport. *J. Atmos. Sol. Terr. Phys.* 104: 116-125.

Arya, P.S. 2001. *Introduction to micrometeorology* (2nd Ed.). Academic Press, United States of America, 390p.

Arya, P. S. 2005. Micrometeorology and atmospheric boundary layer. *Pure Appl. Geophys.* 162(10): 1721-1745.

Babu, S.S. and Moorthy, K.K. 2002. Aerosol black carbon over a tropical coastal station in India. *Geophys. Res. Lett.* 29(23): 13-1-13-4.

Beegum, S.N., Moorthy, K.K., Babu, S.S., Satheesh, S.K., Vinoj, V., Badarinath, K.V.S., Safai, P.D., Devara, P.C.S., Singh, S., Dumka, U.C., and Pant, P. 2009. Spatial distribution of aerosol black carbon over India during pre-monsoon season. *Atmos. Environ.* 43(5): 1071-1078.

Begam, G.R., Vachaspati, C.V., Ahammed, Y.N., Kumar, K.R., Babu, S.S., and Reddy, R.R. 2016. Measurement and analysis of black carbon aerosols over a tropical semi-arid station in Kadapa India. *Atmos. Res.* 171: 77-91.

Bhat, G.S. and Arunchandra, S.C. 2008. On the measurement of the surface energy budget over a land surface during the summer monsoon. *J. earth syst. Sci.* 117(6): 911-923.

Bierly, E.W. and Hewson, E.W. 1962. Some restrictive meteorological conditions to be considered in the design of stacks. *J. Appl. Meteor.* 1(3): 383-390.

Bond, T.C., Doherty, S.J., Fahey, D.W., Forster, P.M., Berntsen, T., DeAngelo, B.J., Flanner, M.G., Ghan, S., Kärcher, B., Koch, D., and Kinne, S. 2013. Bounding the role of black carbon in the climate system: A scientific assessment. *J. Geophys. Res. Atmos.* 118(11): 5380-5552.

Boucher, O., Randall, D., Artaxo, P., Bretherton, C., Feingold, G., Forster, P., Kerminen, V.M., Kondo, Y., Liao, H., Lohmann, U., Rasch, P., Satheesh S.K., Sherwood, S., Stevens, B., and Zhang., X.Y. 2013. Clouds and Aerosols. In: Climate Change 2013: The Physical Science Basis. Contribution of Working Group I to the Fifth Assessment Report of the Intergovernmental Panel on Climate Change [Stocker, T.F., D. Qin, G.-K. Plattner, M. Tignor, S.K. Allen, J. Boschung, A. Nauels, Y. Xia, V. Bex and P.M. Midgley (eds.)]. Cambridge University Press, Cambridge, United Kingdom and New York, USA.

Burns, S.P., Horst, T.W., Jacobsen, L., Blanken, P.D., and Monson, R.K. 2012. Using sonic anemometer temperature to measure sensible heat flux in strong winds. *Atmos. Meas. Tech.* 5(9): 2095.

Change, I.C., 2007. The physical science basis.

Charlson, R.J., Schwartz, S.E., Hales, J.M., Cess, R.D., Coakley, J.J., Hansen, J.E., and Hofmann, D.J. 1992. Climate forcing by anthropogenic aerosols. *Sci.* 255(5043): 423-430.

Drinovec, L., Močnik, G., Zotter, P., Prévôt., A.S.H., Ruckstuhl, C., Coz, E., Rupakheti, M., Sciare, J., Müller, T., Wiedensohler, A., and Hansen, A.D.A. 2015. The" dual-spot" Aethalometer: an improved measurement of aerosol

black carbon with real-time loading compensation. *Atmos. Meas. Technol.* 8: 1965-1979.

Dumka, U.C., Manchanda, R.K., Sinha, P.R., Sreenivasan, S., Moorthy, K.K., and Babu, S.S. 2013. Temporal variability and radiative impact of black carbon aerosol over tropical urban station Hyderabad. *J. Atmos. Sol. Terr. Phys.* 105: 81-90.

Dumka, U.C., Moorthy, K.K., Hegde, P.R.K., Pant, P., Singh, N., and Babu, S.S. 2010. Characteristic aerosol black carbon mass concentrations over a high altitude location in the Central Himalayas from multi-year measurements. *Atmos. Res.* 96(4): 510–521.

Geernaert, G. 2003. Surface layer. *Encyclopedia Atmos. Sci.* Elsevier Academic Press, Amsterdam. 305–311.

Holzworth, G. C. 1967. Mixing depths, wind speeds and air pollution potential for selected locations in the United States. *J. appl. Meteorol.* 6(6): 1039-1044.

Jacobson, M. Z. 2001. Strong radiative heating due to the mixing state of black carbon in atmospheric aerosols. *Nat.* 409: 695-697.

Jacob, D.J. and Winner, D.A. 2009. Effect of climate change on air quality. *Atmos. Environ.* 43(1): 51-63.

Kaimal, J.C. and Finnigan, J.J. 1994. *Atmospheric boundary layer flows: their structure and measurement.* Oxford university press, New York. 289p.

Kipp and Zonen, 2009. Instruction manual, CNR 4 net radiometer. Manual version 1107. Delft, Netherlands.

Kompalli, S.K., Babu, S.S., Moorthy, K.K., Manoj, M.R., Kumar, N.K., Shaeb, K.H.B., and Joshi, A.K. 2014. Aerosol black carbon characteristics over Central India: Temporal variation and its dependence on mixed layer height. *Atmos. Res.* 147: 27-37.

Krishnan, P. and Kunhikrishnan, P.K. 2004. Temporal variations of ventilation coefficient at a tropical Indian station using UHF wind profiler. *Curr. Sci.* 86(3): 447-450.

Kumar, K.R., Narasimhulu, K., Balakrishnaiah, G., Reddy, B.S.K., Gopal, K.R., Reddy, R.R., Satheesh, S.K., Moorthy, K.K., and Babu, S.S. 2011.

Characterization of aerosol black carbon over a tropical semi-arid region of Anantapur, India. *Atmos. Res.* 100(1): 12-27.

Li, Z., Guo, J., Ding, A., Liao, H., Liu, J., Sun, Y., Wang, T., Xue, H., Zhang, H., and Zhu, B. 2017. Aerosol and boundary-layer interactions and impact on air quality. *Natl. Sci. Rev.* 4(6): 810-833.

Mahalakshmi, D.V., Badarinath, K.V.S., and Naidu, C.V. 2011. Influence of Boundary Layer Dynamics on Pollutant Concentrations over Urban Region – A Study Using Ground Based Measurements. *Indian J. Radio Space Phys.* 40: 147–152.

Moorthy, K.K. and Babu, S.S. 2006. Aerosol black carbon over Bay of Bengal observed from an island location, Port Blair: Temporal features and long-range transport. *J. Geophys. Res. Atmos.* 111(D17).

Mues, A., Rupakheti, M., Münkel, C., Lauer, A., Bozem, H., Hoor, P., Butler, T. and Lawrence, M.G., 2017. Investigation of the mixing layer height derived from ceilometer measurements in the Kathmandu Valley and implications for local air quality. *Atmos. Chem. Phys.* 17: 8157-8176.

Murty, K.V., Viswanadham, D.V., and Sadhuram, Y. 1980. Mixing heights and ventilation coefficients for urban centres in India. *Bound.-Layer Meteorol.* 19(4): 441-451.

Nair, V.S., Moorthy, K.K., Alappattu, D.P., Kunhikrishnan, P.K., George, S., Nair, P.R., Babu, S.S., Abish, B., Satheesh, S.K., Tripathi, S.N., and Niranjan, K. 2007. Wintertime aerosol characteristics over the Indo-Gangetic Plain (IGP): Impacts of local boundary layer processes and long-range transport. *J. Geophys. Res. Atmos*.

Nair, S.K., Anurose, T.J., Subrahamanyam, D.B., Kumar, N.V.P., Santosh, M., Sijikumar, S., Mohan, M. and Namboodiri, K.V.S., 2011. Characterization of the Vertical Structure of Coastal Atmospheric Boundary Layer over Thumba (8.5° N, 76.9° E) during Different Seasons. *Adv. in Meteorol.*

Nemmar, A., Hoet, P.M., Vanquickenborne, B., Dinsdale, D., Thomeer, M., Hoylaerts, M.F., Vanbilloen, H., Mortelmans, L., and Nemery, B. 2002.

Passage of inhaled particles into the blood circulation in humans. *Circulation,* 105(4): 411-414.

Nieuwstadt, F.T.M. and Duynkerke, P.G. 1996. Turbulence in the atmospheric boundary layer. *Atmos. Res.* 40(2-4): 111-142.

Oke, T. R. 1978. *Boundary layer climates*. Methuen & Co. Ltd, New York.

Pant, P., Hegde, P., Dumka, U.C., Sagar, R., Satheesh, S.K., Moorthy, K.K., Saha, A., and Srivastava, M.K. 2006. Aerosol characteristics at a high-altitude location in central Himalayas: Optical properties and radiative forcing. *J. Geophys. Res. Atmos.* 111(D17).

Pathak, H.S., Sreedharan, K.S., Nanjundiah, R.S., Moorthy, K.K., Lakshmivarahan, S. and Babu, S.N.S., 2019. Assessment of regional aerosol radiative effects under the SWAAMI campaign–Part 1: Quality-enhanced estimation of columnar aerosol extinction and absorption over the Indian subcontinent. *Atmos. Chem. Phys.* 19(18): 11865-11886.

Patil, M.N., Patil, S.D., Waghmare, R.T., and Dharmaraj, T. 2013. Planetary boundary layer height over the Indian subcontinent during extreme monsoon years. *J. atmos. Sol.-terr. Phys.* 92: 94-99.

Platt, U., Pfeilsticker, K., and Vollmer, M. 2007. *Rad. Opt. Atmos.* 1165p.

Pöschl, U. 2005. Atmospheric aerosols: composition, transformation, climate and health effects. Angewandte Chemie International Ed. 44(46): 7520-7540.

Prospero, J.M., Charlson, R.J., Mohnen, V., Jaenicke, R., Delany, A.C., Moyers, J., Zoller, W., and Rahn, K. 1983. The atmospheric aerosol system: An overview. *Rev. Geophys.* 21(7): 1607-1629.

Ramanathan, V. and Carmichael, G., 2008. Global and regional climate changes due to black carbon. *Nat. geosci.* 1(4): 221-227.

Sandeep, A., Rao, T.N., Ramkiran, C.N., and Rao, S.V.B. 2014. Differences in atmospheric boundary-layer characteristics between wet and dry episodes of the Indian summer monsoon. *Bound.-layer meteorol.* 153(2): 217-236.

Santanello Jr, J.A., Friedl, M.A., and Kustas, W.P. 2005. An empirical investigation of convective planetary boundary layer evolution and its relationship with the land surface. *J. Appl. Meteorol.* 44(6): 917-932.

Sarkar, C., Chatterjee, A., Singh, A.K., Ghosh, S.K., and Raha, S. 2014. Characterization of black carbon aerosols over Darjeeling-A high altitude Himalayan station in eastern India. *Aerosol Air Qual. Res.* 15(2): 465-478.

Satheesh, S.K., 2002. Aerosols and climate. *Resonance,* 7(4): 48-59.

Satheesh, S.K., Krishna Moorthy, K. and Srinivasan, J., 2004. Introduction to Aerosols and Impacts on Climate: Basic Concepts. ISRO GBP Scientific report.

Satheesh, S.K., Moorthy, K.K., Babu, S.S., and Srinivasan, J. 2013. Unusual aerosol characteristics at Challakere in Karnataka. *Curr. Sci.* 104(5): 615-621.

Sathyanadh, A., Prabhakaran, T., Patil, C. and Karipot, A. 2017. Planetary boundary layer height over the Indian subcontinent: Variability and controls with respect to monsoon. *Atmos. Res.* 195: 44-61.

Seinfeld, J.H. and Pandis, S.N. 2016. Atmospheric chemistry and physics: from air pollution to climate change. John Wiley & Sons.

Singh, R.K. and Pandya, G.H. 2013. Atmospheric Mixing-Height Measurements and Ambient Air Quality Near a Coastal Industrial Area: A Case Study From Mangalore. *Environ. Qual. Management,* 22(4): 61-78.

Solomon, S., Qin, D., Manning, M., Chen, Z., Marquis, M., Averyt, K. B., Tignor, M., and H.L. Miller. 2007. Climate Change 2007: The Physical Science Basis. Cambridge, United Kingdom and New York, NY, USA: Cambridge University Press.

SPSS tutorials, (n.d.) Pearson Correlations – Quick Introduction [online]. https://www.spss-tutorials.com/pearson-correlation-coefficient/ [Accessed on 15 August 2020].

Stull, R.B., 1988. *An introduction to boundary layer meteorology*. Kluwer Academic Publishers.

Stull, R. B. 1997. *An Introduction to Boundary Layer Meteorology*. Kluwer Academic Publishers, Boston.

Tiwari S., Srivastava, A.K., Bisht, D.S., Parmita, P., Srivastava, M.K., and Attri, S.D. 2013. Diurnal and seasonal variations of black carbon and PM2.5 over New Delhi, India: Influence of meteorology. *Atmos. Res.* 125–126, 50–62.

Warhaft, Z., 2000. Passive scalars in turbulent flows. *Annu. Rev. of Fluid Mech.* 32(1): 203-240.

Weingartner, E., Saathoff, H., Schnaiter, M., Streit, N., Bitnar, B., and Baltensperger, U. 2003. Absorption of light by soot particles: determination of the absorption coefficient by means of aethalometers. *J. Aerosol Sci.* 34(10): 1445-1463.

Winker, D.M., Pelon, J., Coakley Jr, J.A., Ackerman, S.A., Charlson, R.J., Colarco, P.R., Flamant, P., Fu, Q., Hoff, R.M., Kittaka, C., and Kubar, T.L. 2010. The CALIPSO mission: A global 3D view of aerosols and clouds. *Bulletin of the American Meteorol. Soc.* 91(9): 1211-1230.

Wood, C.R. 2007. The biometeorology of high-altitude insect layers. Ph. D. thesis.

Xiang, Y., Zhang, T., Liu, J., Lv, L., Dong, Y., and Chen, Z. 2019. Atmosphere boundary layer height and its effect on air pollutants in Beijing during winter heavy pollution. *Atmos. Res.* 215: 305-316.

Yu, H., Liu, S.C., and Dickinson, R.E. 2002. Radiative effects of aerosols on the evolution of the atmospheric boundary layer. *J. Geophys. Res. Atmos.* 107(D12): AAC-3.

INVESTIGATIONS ON THE ROLE OF ATMOSPHERIC BOUNDARY LAYER DYNAMICS IN MODULATING THE AIR QUALITY

by

AMRUTHA M. S.

(2015 - 20 - 006)

ABSTRACT

Submitted in the partial fulfilment of the

requirements for the degree of

BSc.-MSc. (Integrated) Climate Change Adaptation

Faculty of Agriculture

Kerala Agricultural University

ACADEMY OF CLIMATE CHANGE EDUCATION AND RESEARCH

VELLANIKKARA, THRISSUR – 680 656

KERALA, INDIA

2020

ABSTRACT

Year-round continuous and collocated measurement of near-surface aerosol black carbon (BC) and atmospheric boundary layer (ABL) parameters has been carried out from the climate observatory located at the second campus of Indian Institute of Science (IISc) at a semi-arid, inland location in southern India, Challakere (14.3° N, 76.6° E, ~580 m amsl) for the period March 2018 – February 2019, to investigate the role of ABL dynamics in modulating the aerosol BC concentration (thereby on the air quality). The semi-arid terrain (ows to the higher convective lifting time) altogether with abundant sub-micron particles point to Challakere being an ideal choice to study the air quality. Significant diurnal variation was shown by BC during ON and DJF season with a sharp shoot during the morning hours (within one hour after sunrise). BC mass concentration was found to be highest (2.65 ± 0.42 μg m^{-3}) during DJF (December, January, and February), moderate in MAM (1.77 ± 0.18 μg m^{-3}) (March, April, and May), and ON (1.58 ± 0.24 μg m^{-3}) (October and November), and extremely lowest during JJAS (June, July, August, and September) (0.30 ±0.02 μg m^{-3}), seasons respectively. These diurnal and seasonal variation were closely associated with the local ABL dynamics and anthropogenic activities. Lowest BC concentration during JJAS accounts for the rainfall events as a part of summer monsoon. MLH (mixed layer height) estimates during clear sky days were only used in the present study, as it ensures a fully evolved ABL with vigorous turbulent mixing. BC concentration have a strong inverse relationship between MLH and VC (ventilation coefficient). Due to high MLH and VC values during MAM season, the dispersion will be greater and thus the air quality is reported to be better as compared to ON and DJF seasons.